Lawrence Berkeley National Laboratory
Recent Work

Title
DECAY OF THE Zn64* COMPOUND NUCLEUS FORMED BY NUCLEAR REACTIONS OF p,He3, He4, AMD C12 WITH Cu63, Ni , Ni61, AND Cr52, RESPECTIVELY

Permalink
https://escholarship.org/uc/item/3wz0x4cp

Author
Smith, Charles F.

Publication Date
1965

eScholarship.org Powered by the California Digital Library
University of California

UCRL-11862

University of California

Ernest O. Lawrence Radiation Laboratory

TWO-WEEK LOAN COPY

This is a Library Circulating Copy which may be borrowed for two weeks. For a personal retention copy, call Tech. Info. Division, Ext. 5545

DECAY OF THE Zn^{64*} COMPOUND NUCLEUS FORMED BY NUCLEAR REACTIONS OF p, He^3, He^4, AND C^{12} WITH Cu^{63}, Ni^{61}, Ni^{60}, AND Cr^{52}, RESPECTIVELY

Berkeley, California

DISCLAIMER

This document was prepared as an account of work sponsored by the United States Government. While this document is believed to contain correct information, neither the United States Government nor any agency thereof, nor the Regents of the University of California, nor any of their employees, makes any warranty, express or implied, or assumes any legal responsibility for the accuracy, completeness, or usefulness of any information, apparatus, product, or process disclosed, or represents that its use would not infringe privately owned rights. Reference herein to any specific commercial product, process, or service by its trade name, trademark, manufacturer, or otherwise, does not necessarily constitute or imply its endorsement, recommendation, or favoring by the United States Government or any agency thereof, or the Regents of the University of California. The views and opinions of authors expressed herein do not necessarily state or reflect those of the United States Government or any agency thereof or the Regents of the University of California.

UCRL-11862

UNIVERSITY OF CALIFORNIA

Lawrence Radiation Laboratory
Berkeley, California

DECAY OF THE Zn^{64*} COMPOUND NUCLEUS FORMED BY NUCLEAR REACTIONS OF p, He^3, He^4, AND C^{12} WITH Cu^{63}, Ni^{61}, Ni^{60}, AND Cr^{52}, RESPECTIVELY

Charles F. Smith, Jr.

(Ph.D. Thesis)

January 1965

DECAY OF THE Zn^{64*} COMPOUND NUCLEUS FORMED BY NUCLEAR REACTIONS OF p, He^3, He^4, AND C^{12} WITH Cu^{63}, Ni^{61}, Ni^{60}, AND Cr^{52}, RESPECTIVELY

Contents

DECAY OF THE Zn^{64*} COMPOUND NUCLEUS FORMED BY NUCLEAR REACTIONS OF p, He^3, He^4, AND C^{12} WITH Cu^{63}, Ni^{61}, Ni^{60}, AND Cr^{52}, RESPECTIVELY

Charles F. Smith, Jr.

Lawrence Radiation Laboratory and Department of Chemistry
University of California
Berkeley, California

January 1965

ABSTRACT

An experimental, radio-chemical determination of the excitation functions for reactions involving the $[Zn^{64}]^*$ compound nucleus has been performed. The reactant pairs are: p + Cu^{63}, He^3 + Ni^{61}, He^4 + Ni^{60}, and C^{12} + Cr^{52}, while the observed products for each such pair are: Zn^{63}, Zn^{62}, and Cu^{62}. Total reaction cross sections are calculated from the optical model. The ratio of the cross section for a given reaction to the total reaction cross section are compared on an excitation energy abscissa for each product. The shape and magnitude of these ratio curves is essentially constant in each such comparison, suggesting a compound nuclear reaction mechanism. Range measurements for Zn^{62} recoils are made and compared to calculated ranges based on the theory of Lindhard, Scharff and Schiøtt for a compound nuclear reaction. Good agreement is found. The shapes of these curves are compared to a theoretical estimate obtained from evaporation theory, and are shown to be similar to the calculated shapes. A displacement of the experimental curves relative to one another along the excitation energy axis is noted, and ascribed to angular momentum effects. Using the position of the Zn^{64} photoexcitation curves of Sagane as reference points, and spin averaged angular momenta of the compound system, the reduced moment of inertia is calculated for the four systems. At least two distinct values are found, indicating a difference between orbital- and spin-angular momenta, the latter causing the greater energy shift in the excitation functions. This observation is shown to be of value in understanding similar energy discrepancies in excitation function comparisons. Because of the observed relationship between the mode of formation and the mode of decay of the compound nucleus, it is concluded that the independence postulate is not strictly applicable to this system as a whole.

I. INTRODUCTION

One of the more interesting developments in the field of nuclear physics during the years following Chadwick's discovery of the neutron[1] was the unusually narrow resonance widths for neutron absorption. According to the uncertainty principle, this implied a very long lifetime for the excited levels and the theory of the day was not adequate to explain this phenomenon. That is, not until 1936 when Bohr suggested the compound nucleus mechanism[2] based on the liquid drop model of the nucleus. According to this picture, target and projectile merge, whereupon the strongly interacting nuclear forces rapidly distribute the excitation energy among all particles in the nucleus. It is quite likely that a good deal of time, on the nuclear scale, will pass before a particle again has enough energy to break the nuclear bonds and escape. Thus, Bohr accounted for the long delay implied by narrow resonance widths with a model analogous to a molecule evaporating from a (hot) liquid drop.

Bohr's simple concept has been converted into a method for statistical analysis of nuclear reactions by Weisskopf.[3] Since then the theoretical treatment has been expanded and developed by several authors.[4-8] Bodansky[9] recently published a comprehensive review of the state of the art for compound-statistical nuclear reactions. A summary of statistical theory as it pertains to this work is included as part of Sec. III.

A major consequence of compound nucleus theory is its prediction that the mode of formation of the compound system should not effect its mode of decay. This concept was first tested by Ghoshal[10] who formed the compound nucleus $[Zn^{64}]^*$ by bombarding Ni^{60} with alpha particles and Cu^{63} with protons. Comparison of the (x,n), (x,2n), and (x,pn) excitation functions on an adjusted energy scale showed remarkable similarity between the curves for a given product. Ghoshal's curves are reproduced in Fig. 1. These experiments have been repeated by Meadows[11] and Tanaka,[12] and portions of the energy range covered by Ghoshal have been re-investigated by several experimenters.[13-15] Figure 2, after Tanaka,[12] collects these determinations for comparison.

From examination of Ghoshal's curves and those of other experimenters, several discrepancies become apparent. It is clear that Ghoshal's

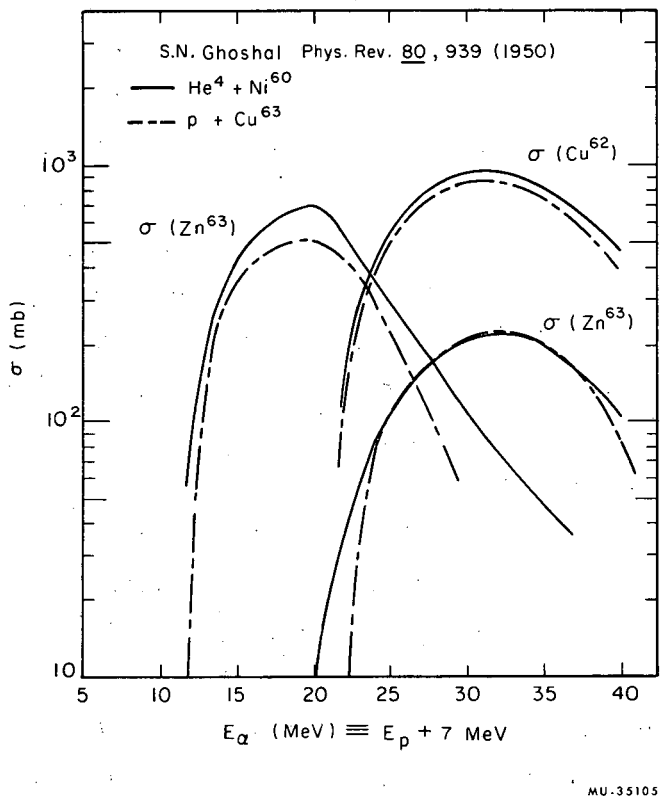

Fig. 1. Experimental excitation functions of S. N. Ghoshal for the He^4 + Ni^{60} and p + Cu^{63} reactions, adapted from ref. 10.

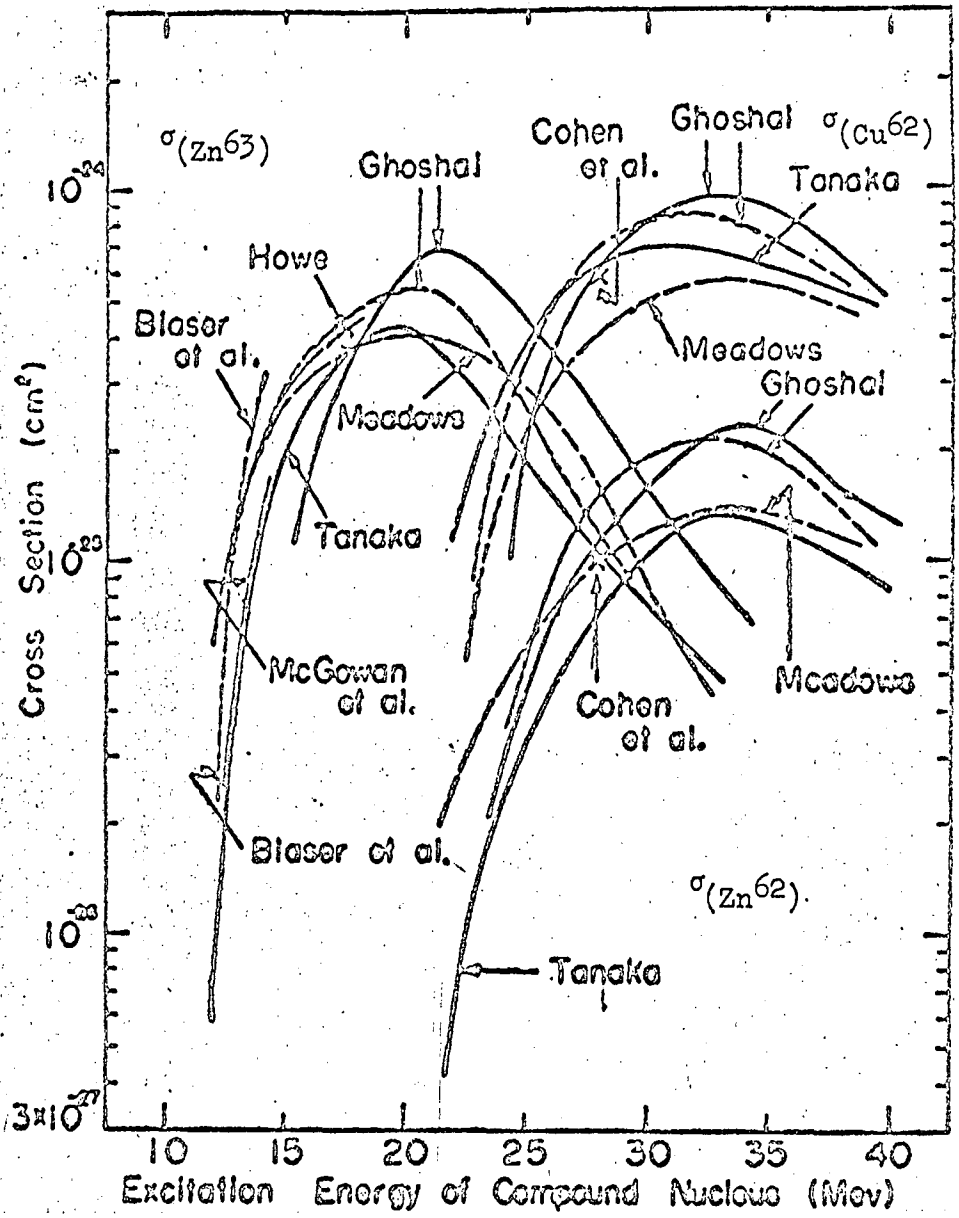

Fig. 2. Collection of available data for comparison between the alpha-particle reactions with Ni^{60} (solid lines) and the proton reactions with Cu^{63} (dashed curves). Curves after Tanaka, ref. 12.

Reaction	Bombarding Energy	Author	Reference
$Ni^{60} + \alpha$	40 and 32 MeV	Tanaka	12
$Ni^{60} + \alpha$	40	Ghoshal	10
$Ni^{60} + \alpha$	11.0	McGowan et al.	13
$Cu^{63} + p$	32	Ghoshal	10
$Cu^{63} + p$	100 and 75	Meadows	11
$Cu^{63} + p$	12	Howe	14
$Cu^{63} + p$	6.7	Blaser et al.	15
$Cu^{63} + p$	21.5	Cohen et al.	16

curves are higher and of a slightly different shape than the consensus of the more recent work. Furthermore, there appears to be a difference in position between curves for a given product when they are plotted vs calculated excitation energy, represented by the difference between the experimental 7 MeV used by Ghoshal and the calculated value. Therefore, a re-examination of this system appears to be of value. It is of importance to re-determine the excitation functions for these reactions in order that the magnitude may be fixed. This is especially desirable at higher energies where only two, rather differing, values of these functions have been determined. The energy shift is also of interest. If real, it must be explained and if not, a re-examination may show that it is not. John's mass considerations do establish that the observed shift (Ghoshal's) is outside experimental error.[17]

Several experimenters have applied a Ghoshal-type test to excitation functions for formation of the same compound nucleus in a series of reactions.[18-28] These observations and their relationship to the present work are reviewed in fair detail in Sec. IV of this dissertation. However, several general conclusions can be made here. In all the results of which the author is aware, the gross shape of corresponding excitation functions is quite similar. There are, to be sure, examples in which the compound nucleus concept is only a portion of the total mechanism, but even in these cases the Ghoshal type test is fulfilled. Comparison of "iso-compound-nuclear" curves on an excitation energy basis paints a rather confusing picture, however. There appears to be a shift, but its magnitude and even its direction is in doubt. The more recent authors[16,24,25,27,29,30] attribute this energy discrepancy to angular momentum effects, but there is no agreement on how best to estimate its magnitude or even to correlate the experimental observations.

Thus, the present work has two main purposes: first, to re-examine the Ghoshal experiment in an attempt to extract as much additional information as possible, and second, to attempt to explain these results in terms which will also bring order to the rather confusing results for other Ghoshal-type experiments. Experimentally, the excitation functions for the series of reactions:

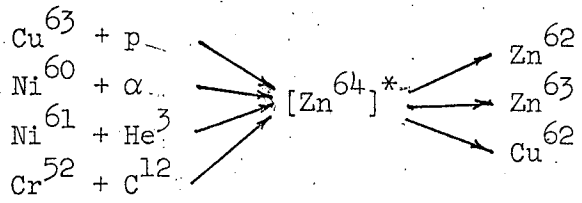

are determined. These results will provide the first four-way test of the independence postulate. Furthermore, the various reactions will produce the compound nucleus with widely differing amounts of angular momenta, thus allowing a quantitative comparison of angular momentum effects on the decay of the excited system. The insight thus gained will be applied to other "iso-compound-nuclear" systems with the hope of presenting a unified picture of this family of experiments.

II. EXPERIMENTAL PROCEDURES

During the course of this work excitation functions for the reactions $p + Cu^{63}$, $\alpha + Ni^{60}$, $He^{3} + Ni^{61}$ and $C^{12} + Cr^{52}$ were determined for production of Zn^{62}, Zn^{63}, and Cu^{62}. Projectile beams were allowed to impinge upon the target. The beam was degraded by aluminum foils until it reached the desired energy and then was allowed to strike a thin metal target. Immediately "behind" the target foil, a catcher foil was included. Normally several such degrader-target-catcher units were stacked in a single target holder, the actual number of targets being governed by the desired energy for each foil and the technique to be used later in counting them.

Following some bombardments, the target foils and their catcher foils were mounted separately on 1/16-inch aluminum cards and placed under an end-window β proportional counter. (This group of experiments will henceforth be referred to as the direct counting group.) Each counter was equipped with an automatic timer-printer (pipper) which could be set to record counts at any desired interval (up to 100 minutes). By decreasing the scaling factor of the counters and increasing the time between counts (pips), reasonably good counting statistics were obtained throughout the counting period. The pipper record yielded decay data which were then resolved by half lives.

In a second group of experiments (the chemically separated group) the target foils were dissolved in concentrated HCl containing 10 mg of each of the appropriate carriers, and the copper and zinc fractions were isolated by conventional radiochemical procedures. These fractions were precipitated, deposited on filter paper disks, mounted on aluminum cards and counted in the same manner described above for the direct counting group.

Because of the greater complexity of the decay curves obtained by direct counting, the resultant analysis suffered somewhat in accuracy. On the other hand the chemically separated samples suffered from the uncertainty of chemical analysis. These two sets of experiments are complimentary in the sense that they may be used to check each other.

Furthermore, the conditions imposed by the experimental arrangement often dictated which of the two counting procedures should be used. (E.g., at high energies of bombardment the direct counting decay curves are quite complex due to the greater number of reactions that took place with both target and catcher foils. Therefore, most of the high energy experiments are in the chemically separated group.)

Decay curve analysis for the more complex curves was accomplished with the aid of the IBM 704, 709, or 7090 computers (whichever was available at the time). The program, FRENIC, gives an iterative, least squares fit to decay curves with up to ten components.[31] Less complex direct counting curves and most of the chemically separated curves were analyzed by hand. The result of either method is a set of counting rates, A_0, at end of bombardment for the various components. Experimental detection coefficients using published branching ratios, and chemical yield values, where appropriate, were used to convert the A_0's to absolute disintegration rates at time equal zero, D_0, according to Eq. 1.

$$D_0 = A_0/(ODC)(Y) \tag{1}$$

where ODC = overall detection coefficient (described in Appendix V)

Y = chemical yield (Y = 1 for direct counting experiments).

The cross sections were then calculated using the formula:

$$\sigma_{(E)} = \frac{D_0}{nI\,(1 - e^{-\lambda\tau})} \tag{2}$$

where $\sigma_{(E)}$ = cross section at a given energy in cm^2 per atom

D_0 = disintegration rate at time zero, in disintegrations per minute

n = number of target atoms per cm^2

τ = length of bombardment in minutes

λ = decay constant in $(minutes)^{-1}$

I = total number of bombarding particles/τ, ions per minute.

For a few experiments the accelerator beam could not be considered constant. In these instances the cross section was calculated from a modified form of Eq. 2:

$$\sigma_{(E)} = D_0/n\ \lambda \cdot \sum_i I_i\ e^{-\lambda(t_0-\Delta t)} \qquad (3)$$

This amounts to a sum of cross sections over an interval Δt, which is less than τ and small compared to the half lives being considered.

Details of these various experimental procedures are described in the following sections.

A. Target Preparation

Natural copper foils were used as the target material for the $p + Cu^{63}$ bombardments. These high-purity foils were obtained from the Chromium Corporation of America in the form of one-inch squares and were nominally 0.125 mil (~ 3 mg/cm^2) thick. From these a 7/8-inch diameter circular foil was punched for use as the target. The true thickness was then determined by weighing on a torsion balance.

Proton energy loss is small in passing through foils of this thickness so that three target foils were employed at each energy rather than a single target foil as described below in the cases of heavier projectiles. Only the center foil of this target sandwich was counted since, because of the negligible beam degradation, it is possible to make the assumption that products recoiling into the center foil are evenly balanced by products recoiling out of this foil. It is only necessary to choose foils of sufficient thickness to prevent recoils from passing completely through a foil to satisfy this approximation. With the aid of recoil range-energy curves (discussed in Sec. II-C), the present thickness was chosen as being sufficient to stop more than 99% of the recoils from proton reactions with target (or degrader) material. The result is an isolated target foil which contains only products of the $p + Cu^{63,65}$ reactions. The Cu^{63} abundance was 69.09%.

The nickel targets for use in the $Ni^{60} + \alpha$ reaction studies were high-purity natural nickel foils. These foils also were supplied by

Chromium Corporation of America in the form of one-inch squares and were nominally 0.175 mil (3mg/cm^2) thick. From these a circular foil of 7/8-inch diameter was punched. The true thickness was then determined by weighing. Natural nickel is 26.16% Ni^{60}. In most experiments 1/4 mil (1.7 mg/cm^2) aluminum was used as a catcher foil, the catcher foil for the remainder being 1/2 mil (3.4 mg/cm^2) aluminum.

Targets for the Ni^{61} + He^3 experiments were prepared by electrodeposition of enriched Ni^{61} obtained from Oak Ridge, onto 1/4 mil (12 mg/cm^2) gold foils. Plating was carried out from a basic solution containing the Ni^{61} as the ammonia complex. The cell was designed to incorporate the gold backing foil as the cathode and to confine the nickel deposit to a circular area 5/8-inch in diameter. Preliminary experiments indicated that under the conditions of this plating, the deposit was uniform to ± 5%. Target thickness was calculated from the difference in weight of the gold backing foil before and after electroplating. Three such targets were prepared, two of which were 1.55 ± 0.07 mg/cm^2 (~ 0.07 mil) while the third was about half that thick (0.74 mg/cm^2). For these experiments the gold back served not only to support the nickel deposit, but also as the catcher foil. These targets were used throughout the series of bombardments and were not subjected to further chemical action.

The chromium targets were also prepared by electrodeposition. Since the natural isotopic abundance of Cr^{52} is 83.76% separated isotopes were not required. Plating was performed according to the industrial recipe,[32] using a chromic acid—sulphuric acid mixture. As with the nickel plating, gold foils were chosen as backing material, but 1/10 mil (5mg/cm^2) gold was sometimes used instead of 1/4 mil as in the previous case. The gold foil was incorporated into the cathode in such a way as to expose a circular area 13/16-inch in diameter to the solution. Thickness was calculated from the difference in weights before and after plating. Uniformity was experimentally checked and found to be satisfactory (± 5%). Target thicknesses varied, but a typical value would be about 1.2 mg/cm^2.

Details of the procedures used in target preparation and electrodeposition of nickel and chromium are included in Appendix I. A description of preliminary experiments to test uniformity and to optimize the

procedures is also included. The chemical composition and mass analysis of the targets used in this work are presented in Table 1.

B. Bombardments

The source of protons was the 88-inch spiral ridge cyclotron at Berkeley. A beam of 30.0 ± 0.6 MeV protons was allowed to impinge on the target assembly by adjustment of a series of bending magnets. For those familiar with this machine, the energy uncertainty quoted is an estimate of week-to-week variations in beam energy and does not imply that for a given set of conditions on a given day that the beam energy is this much in doubt. The target holder used is a copper block, water cooled, to which the stack of degrader foils and target sandwiches may be clamped. This holder, when properly shielded by a magnetic field, doubled as the Faraday cup which enabled continuous measurement of the proton beam during bombardment. This target holder, referred to as a Cu-tag, is illustrated in Fig. 3. Typical beam currents were on the order of 0.1 microampere and bombardments lasted from 10 to 15 minutes.

Helium-4 beams from the Berkeley 60-inch cyclotron (now at University of California, Davis) and from the Berkeley Heavy Ion Linear Accelerator (Hilac) were used for the Ni^{60} bombardments. The 60-inch external beam of 48.3 ± 1 MeV[33] alpha particles was used for about half of the total number of such experiments included here. Targets consisted of a stack of aluminum degrader foils with from three to six nickel target foils inserted at depths such that the beam entered each at the desired energy. This stack was clamped in the bottom of a water-cooled copper target holder. The extracted beam was focused and then directed onto the center of the top foil of the stack. The target holder, shielded by magnets, acted as a Faraday cup. Average beams were 250 mμA and normal bombarding times were 10 to 15 minutes. Alpha particles from the Hilac are extracted with an energy of 41.6 MeV (10.4 ± 0.2 MeV/Amu).[34] The Hilac target holder is the same copper-tag target described previously in the section on proton bombardments. Target foils are clamped to the front face and the entire unit is inserted in one of the exit ports of the accelerator. The target make-up was the same for both cyclotron and Hilac

Table I. Chemical composition and mass analysis of target materials.

Target	Chemical impurities (maximum) (percent)		Mass analysis (percent)	
Natural Nickel	>99.4	Ni	67.76	Ni^{58}
	0.53	Co	26.16	Ni^{60}
	0.015	S	1.25	Ni^{61}
	0.009	Cu	3.66	Ni^{62}
	0.013	Fe	1.16	Ni^{64}
	0.001 each	Zn,Pb,Sb,Cd, C,Mn,Mg,Si		
Enriched Nickel-61	0.04	Cu	4.83±0.09	Ni^{58}
	0.04	Fe	7.57±0.11	Ni^{60}
	0.01	Li	79.49±0.21	Ni^{61}
	0.04	Mg	3.58±0.04	Ni^{62}
	0.01	Na	4.54±0.06	Ni^{64}
	0.04	Si		
Natural Chromium	0.03	Fe	4.31	Cr^{50}
	0.03	Al	83.76	Cr^{52}
	0.03	Ba	9.55	Cr^{53}
	0.01	others	2.38	Cr^{54}
Natural Copper	>99.4	Cu	69.06	Cu^{63}
	0.6	Co	30.91	Cu^{65}
	< 0.1	others		

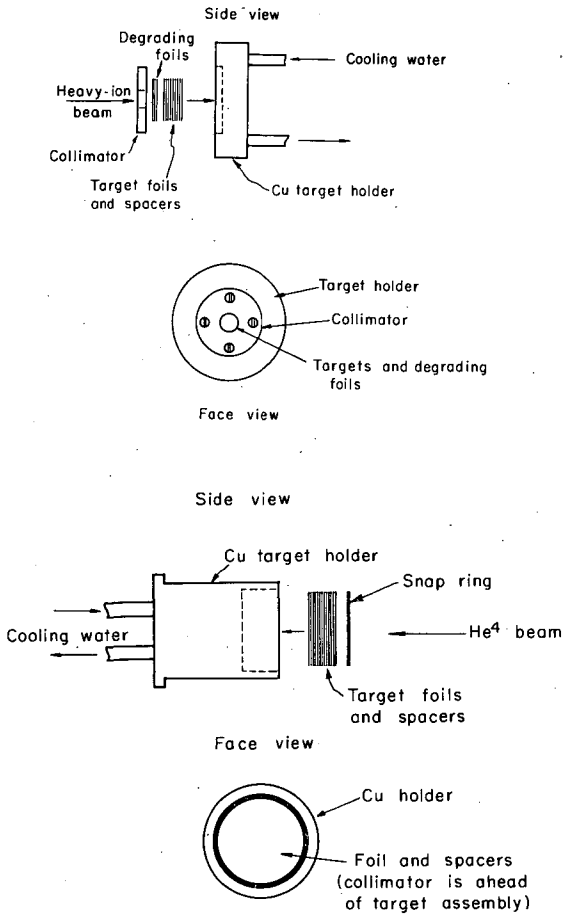

Fig. 3. Target holders used for bombardments. The copper tag target (above) was used for He^3, He^4, and C^{12} bombardments at the Hilac and for proton bombardments at the 88" cyclotron. The cyclotron target (below) was used for He^4 bombardments at the 60" cyclotron.

bombardments. The beam was continuously monitored and recorded on a calibrated electrometer connected to the Faraday cup. Typical beam currents were on the order of 250 to 300 mμA, and bombarding times varied from 10 to 20 minutes.

The Hilac also provided the 30.6 MeV He^3 beam for the Ni^{61} bombardments. The three Ni^{61} targets were interspersed among aluminum degraders at appropriate intervals with the nickel upstream from the gold backing. Thus, the gold served as a catcher foil for the recoil nuclei. This stack was clamped to the face of the copper block and bombarded in the same manner as described above. Beam currents were kept low to avoid overheating of the targets since these foils were to be re-used several times. For this reason beam currents were held below 200 mμA and bombarding times, about 20 minutes, were correspondingly larger than for the alpha particle bombardments.

Carbon ion bombardments of chromium were also made at the Hilac. Physically, the arrangement was identical to that described above. For low energy, direct counting experiments, the gold backing was 1/4 mil thick and served as a recoil catcher foil. At higher energies and where chemically separated samples were counted the gold was placed upbeam and the recoil nuclei were caught in an aluminum foil of suitable thickness (1/4 to 1/2 mil). In these cases 1/10 mil gold was used as a backing for the chromium target. Typically, intensities up to 400 mμA were used and bombarding times ran from 10 to 15 minutes.

All bombardments at the 88-inch cyclotron, Hilac, and some of the 60-inch cyclotron bombardments were preceded by a standardization of the integrating beam electrometer. Details of the procedure for this electrometer calibration are included in Appendix II.

C. Range-Energy Relations

Energy determinations for this work are based upon knowledge of the energy loss of the beam particles in passing through the various materials included in a target stack. Values for the range of protons in aluminum and copper were obtained from Sternheimer's calculations[35] and,

for aluminum, from the experimental values of Bischel.[36] Good agreement is found between these two sources of range-energy relations. Alpha particle and carbon ion ranges used for these determinations are those calculated from stopping power curves in Al, Ni, and Au by Northcliffe.[37] Ranges for carbon ions in Cr were obtained by interpolation and are based on the curves given by Northcliffe for Al and Ni. The empirical tables of Williamson and Boujot[38] were used for the ranges of He^3 in these materials. These sources were chosen because they provide a basically consistent set of curves for the particles and materials used and because they appear to agree well with available experimental data. The He^3 curve in Al as given by Williamson and Boujot is so nearly identical to the corresponding curve presented by Northcliffe that no attempt at intercorrelation needed to be made.

Furthermore, since we are using only differences between values of ranges or energies, any error in the absolute magnitude of the curves would tend to cancel (assuming the "true" curve to be parallel to those actually used). In actuality, such questions are of little importance compared to the uncertainty imparted by beam energy and straggling. The accelerator beams have an initial uncertainty of ~ 2% and in traversing the target stack this will increase considerably. In addition, uncertainties due to the loss of energy as a particle traverses a target foil of finite thickness, and the uncertainty of the foil thickness, itself, are the source of another 2 to 6% error in the energy determinations. Therefore, it is assumed that the energy determinations for each of the four projectiles are as accurate as possible by present standards and that only uncertainties in beam energy and target thickness will be included as sources of error in the experiments.

During the course of this work it was desirable to know the ranges of the recoil nuclei following the nuclear reaction. The formalism of Lindhard, Scharff and Schiøtt[39] was used to estimate these ranges. These authors present a set of universal range energy curves for various values of their electronic stopping parameter, κ, plotted as a function of a dimensionless range, ρ, and a dimensionless energy, ϵ. The calculated relationship between these quantities and conventional ranges and energies

is listed in Table II. Also included in the table are conversion factors which were used to reduce the mean total ranges ($\bar{R}$) to find the mean projected range along the beam direction ($\bar{R}_p$). With these parameters, it is possible to obtain a range energy curve of the conventional type. Recoil energies used here are calculated by assuming isotropic emission of decay particles and compound nuclear (i.e. complete fusion) mechanisms. The energy is given by

$$E_R = \frac{A_P A_R}{(A_P + A_T)^2} E_P \qquad (4)$$

where E = Energy (MeV)

A = Mass number

and subscripts P, R, T refer to projectile, recoil nucleus, and target nucleus respectively. The curves obtained in this manner are shown in Fig. 4.

While these curves are approximations, they are quite useful in estimating thicknesses of catcher foils required, amount of forward scattering from target foils and depth of penetration of recoils. It should be emphasized that these curves are only an estimate of mean ranges of the recoils in various stopping media, and that the distribution of ranges about this average is quite broad. This is primarily due to range straggling. Again referring to Lindhard et al., an approximation of this straggling is seen to approach 41% for A = 62 recoils in nickel, the straggling being somewhat less for other materials. In designing the present experiments, this variation in ranges was allowed for by increasing the thickness of the catcher foils to at least 3 $\bar{R}_p$. For other considerations the use of mean range was justified in spite of this breadth of the range distribution.

D. Chemical Separations

Approximately one-half of the natural nickel and chromium targets were subjected to radiochemical separation following bombardment. Each target and the associated catcher foil were dissolved in concentrated HCl containing 10 mg each of the appropriate carriers.

Table II. Parameters for calculation of range-energy relations for Zn^{62} recoils in various materials.

Matrix	κ	ρ	ϵ	R/R_p
Al	0.12	85.5 R	6.49 E	1.15
Cr	0.15	44.2 R	4.86 E	1.28
Ni	0.16	37.5 R	4.33 E	1.34
Au	0.35	10.6 R	1.68 E	2.46

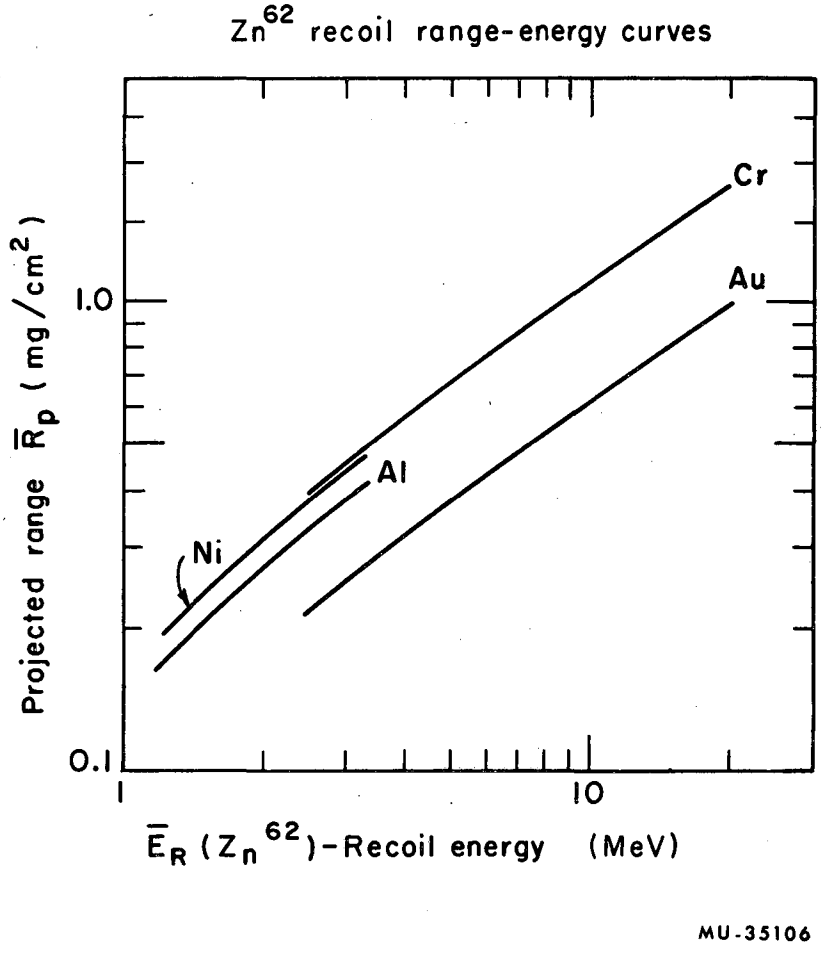

Fig. 4. Calculated range-energy relations for Zn^{62} recoils in various materials.

$Al(OH)_3$ was used as a scavenger to remove unwanted impurities. Copper and zinc fractions were separated in the early work using a Dowex-1 cation exchange column. Later separations used more rapid qualitative analysis methods. The cation exchange method was abandoned because of time considerations. Typical "beam-off to counting" times for chemical separations was 15 minutes while the interval using cation exchange was closer to 30 minutes. (Five to ten minutes were consumed in transit from accelerator to laboratory.)

Copper was separated as the metal, while zinc was obtained as $ZnNH_4PO_4$. These precipitates, representing about 80% chemical yield, were transferred to filter paper disks, washed and mounted for counting. The samples were placed onto the 1/16-inch thick aluminum counting card on top of double-sided cellophane tape. Zapon lacquer (~1/2 mg/cm^2 thickness) was added as a binder. As a further safegaurd against loss and counter contamination, a thin (1 mg/cm^2) film of polystyrene was used as a sample cover. The overall thickness from the view point of the positrons was therefore less than 12 mg/cm^2 for the zinc samples and less than 5 mg/cm^2 for the copper samples. (Sample area ~ 3 cm^2.)

Detailed flow-sheets for the chemistry involved in sample preparation during this work are presented in Appendix III.

E. Counting Procedures

The mounted samples were counted using end-window gas-flow beta proportional counters. These counters were described by Blann[40] and modified by Reeder.[41] The seven β counters used during this work were intercalibrated several times during each experiment, using a Cl^{36} standard, and all counts were adjusted to a constant counting rate for the standard. Such correction was normally on the order of 1 to 2%. Where necessary, resolving time corrections were made. Overall detection coefficients were determined experimentally for each of the isotopes being investigated by comparing the count rate for a pure weightless sample on a 4π counter with the count rate for the same sample, mounted in the standard fashion, on each of several shelves of each beta counter. This

procedure eliminated the need to make separate corrections for back scatter, air absorption, shelf geometry, etc. Self-absorption corrections were quite small and were therefore neglected. This fact, which was checked experimentally using known amounts of each of the radioisotopes and varying amounts of carrier, is due to the rather high energies of the emitted positrons. Properties of the isotopes studied are listed in Table 3. Appendices IV and V describe the determination of the various correction factors.

Measurement of the decay curves was facilitated by use of automatic timing printers which recorded total counts observed in a pre-set time interval, reset, and continued to cycle. During the print cycle, the "pippers" were unable to register input pulses. Often there was a significant dead time and corrections were made to allow for it. The pippers were connected to the mechanical register of the scaling units and the scaling factor applicable to the scaler also controlled the pipper. Scale factors and time intervals could, therefore, be varied throughout the counting period to maintain good counting statistics. The time intervals were also adjusted to provide as many pips as feasible during the half life of the principal component of interest at that moment. It was thus possible to obtain numerous points on the decay curves, to follow these curves for considerable periods of time without the gaps common to manual counting, and to maintain good statistics throughout. Furthermore, the data analysis was made easier and more accurate by virtue of the larger volume of experimental data collected.

F. Data Analysis

The traditional procedures of decay curve analysis were applied to break each experimental curve into its separate components.[45] All decay curves were first analyzed by "hand" to obtain approximate intercepts at time zero for each component. Those curves for which such determinations were unreliable were then subjected to an analysis by computer using the FRENIC program.[31] FRENIC provides a least squares fit to decay curves with up to ten components and has the capability of allowing the slopes to vary or of holding them constant. Computer analysis

Table III. Properties of radioisotopes treated in this experiment.

Isotope	$t_{1/2}$	Positron energies (MeV)	Ref.
Zn^{62}	9.33 h	0.66 [a] (10%)	42
		0.47 (4%)	
		0.92 (0.4%)	
Zn^{63}	38.1 m	1.40 (7%)	43
		1.67 (10%)	
		2.336 (73%)	
		94.4% Total β+	
		1.74 (0.2%)	
Cu^{62}	9.94 m		44
		2.91 (99.8%)	

[a] Zn^{62} is detected primarily through its Cu^{62} daughter.

was necessary for only a limited number of the determinations. Chemical separation reduced the number of components to three in the case of Zn and to three or four (at high energies) in the case of Cu. In every case the components are easily separated due to wide differences in half lives. Even some of the direct counting decay curves proved to be quite easy to analyze. This is true particularly at the lower energies where a typical curve would have only five components. Complications at higher energies because of the increased number of reactions possible were countered with chemical separation and/or computer analysis. Several experiments using each of the target-projectile systems and both counting procedures were computer analyzed to check the accuracy of the preliminary analysis, and in no case were serious discrepancies noted. Accuracies are dependent upon curve complexity for either computer or manual analysis, but in all cases the extrapolated activity at end of bombardment is reliable to less than ± 10%. Typical computer determinations and good manual determinations for moderately complex decay curves averaged about ± 5%. Estimates of error are included in the computer print out. They are made for the manual analyses by moving the experimental line about the "best" value within limits set by the subtractions during analysis. Such errors are cumulative and are, therefore, largest for the shortest lived species.

Once obtained, the A_0's were converted to disintegration rates at time zero, D_0, by application of Eq. 1. Cross sections were then calculated in the manner indicated by Eq. 2 or Eq. 3. Presentation of the results and a discussion of overall errors are the topics for Sec. III of this dissertation.

G. Recoil Experiments

Several measurements relating to the range of product nuclide recoils in aluminum were attempted to supplement the excitation function measurements. Two varieties of range experiments were performed: the thick target type which measures the fraction of recoils escaping the target and the thin target type which measures the range of the recoil atoms in the catcher foils. All these experiments were performed at the

Hilac, using the target holder and bombardment procedures described earlier.

A thick target experiment consists basically of the target foil, thick compared to the range of the recoils, sandwiched between two catcher foils. Because of the nature of these recoil atoms, neutron (or proton) emission could not produce a significant number of backward recoils. (See Experimental Results, Sec. III, for a more complete discussion.) Therefore, in these experiments only the forward recoils were collected. Thus the target assembly consisted of aluminum foils to degrade the beam to the desired energy followed by the target and one or more aluminum catcher foils. For experiments in which the target material was Ni^{61} the target foil was reversed so that the beam passed first through the gold backing material thence into the target itself. The total activity produced is determined by direct counting of the target and catcher foil(s) separately. The fraction recoiling forward is given by the ratio of activity in the catcher(s) to that in both target and catcher(s) ignoring backward scatter.

The thin target experiments are so called because target thickness is reduced to the point that nearly all the recoils escape the target. Therefore in the limit of zero straggling the fraction recoiling forward is unity. In actuality, the spread in ranges about a mean due to straggling is large enough to reduce this fraction somewhat. Nevertheless, for the purposes of these experiments, measurement of the fraction recoiling is not important. The fact that degradation in the target is small allows measurement of the mean range projected on the beam direction by noting the fraction of recoils passing through each foil of a series of thin catcher foils immediately downstream from the target. The more precise the desired measurement the thinner should be the catcher foils. Those selected for this work were aluminum leaf (0.75 ± 0.01 mg/cm^2). Counting was again done without prior chemistry and included the target and several catcher foils. Decay curve analysis removed the chance of including any contributions from reactions other than the reaction being investigated (e.g., $Al^{27}(n,\alpha)Na^{24}$). Procedures for analysis of the data are included in the section presenting the results of these recoil experiments.

III. EXPERIMENTAL RESULTS AND DISCUSSION

During the course of this work absolute values of the cross sections for the reactions

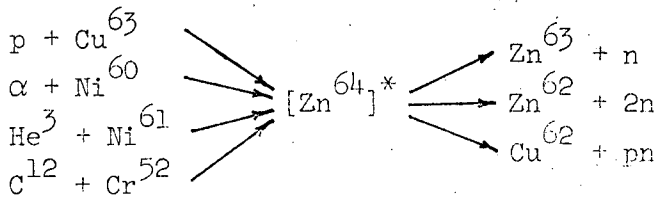

were measured at projectile energies between the Coulomb barrier and 10 MeV per nucleon, or to 30 MeV in the case of p + Cu^{63}. The excitation functions thus obtained constitute the primary experimental results. Of secondary importance, but at the same time serving to support the excitation function measurements, are the results of some extremely rough recoil-range measurements. The excitation functions are presented in Figs. 5,7,9, and 10, and compared to previously published work in Figs. 6 and 8. Typical recoil-range results appear in Figs. 11 and 12. The following paragraphs provide a discussion of the properties of the individual curves. For convenience all appropriate Coulomb barrier energies and reaction Q values are summarized in Table 4.

A. Excitation Function Studies

1. p + Cu^{63}

The existing experimental excitation functions for the (p,n), (p,2n), and (p,pn) reactions[10,11,46] are in reasonably good agreement regarding their position on the energy axis. They do, however, differ in magnitude on the cross section axis. Several experimenters[14,15,16] have measured absolute cross sections for one or more of these reactions at specific energies, but these results do not allow determination of the "best" shape and magnitude of the experimental curves. In order to resolve this uneasy situation these experiments were repeated. Results of the present investigation are shown in Fig. 5 along with the several points determined by other investigators. As is clearly seen, these points

Table IV. Coulomb barriers and Q values for several reactions of interest.

Reaction	Coulomb barrier (MeV)[a]	Q-value (MeV)
$Cu^{63}(p,n)Zn^{63}$		- 4.2
$Cu^{63}(p,2n)Zn^{62}$	5.9	-13.3
$Cu^{63}(p,pn)Cu^{62}$		-10.8
$Ni^{60}(\alpha,n)Zn^{63}$		- 7.0
$Ni^{60}(\alpha,2n)Zn^{62}$	10.2	-17.1
$Ni^{60}(\alpha,pn)Cu^{62}$		-14.6
$Ni^{61}(He^{3},n)Zn^{63}$		+ 4.8
$Ni^{61}(He^{3},2n)Zn^{62}$	10.7	+ 4.3
$Ni^{61}(He^{3},pn)Cu^{62}$		- 1.8
$Cr^{52}(C^{12}.n)Zn^{63}$		- 1.3
$Cr^{52}(C^{12},2n)Zn^{62}$	23.5	-10.4
$Cr^{52}(C^{12},pn)Zn^{63}$		- 8.0

[a] The Coulomb barriers were calculated assuming $r_0 = 1.40$ Fermis.

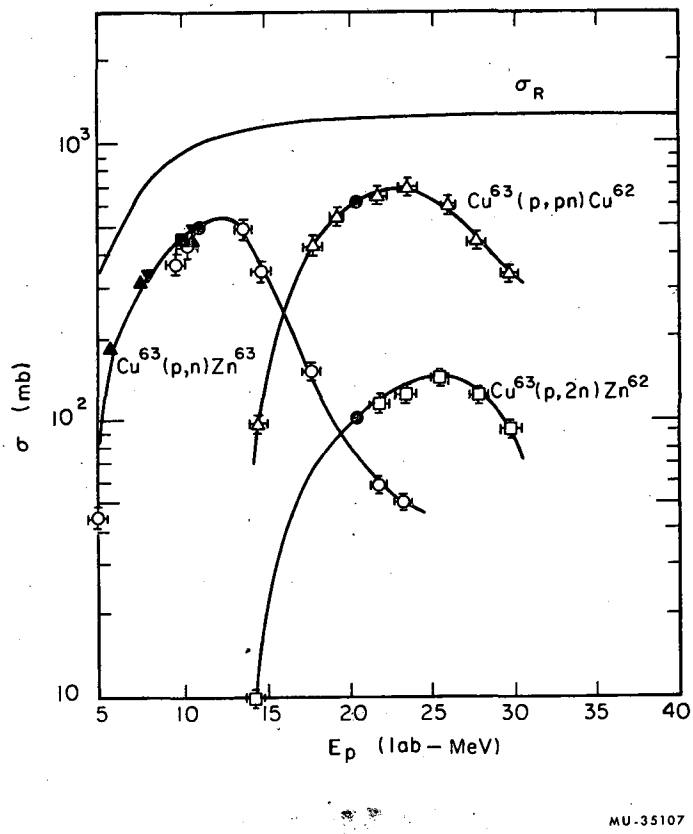

Fig. 5. Experimental excitation functions for p + Cu^{63} reactions, including the total reaction cross section. Present results are indicated by open points. Results of Howe (ref. 14) by ▼, those of Cohen et al. (ref. 16) by ●, those of Albert and Hansen (Phys. Rev. 123, 1749 (1961)) by ■, and those of Wing and Huizenga (Phys. Rev. 128, 280 (1962)) by ▲.

provide a uniform set of data and permit construction of a set of excitation functions. It is these curves that will be used henceforth as the experimental curves for p + Cu^{63} in this discussion.

It is of interest to compare these experimental curves to the previously mentioned curves of Ghoshal and Meadows. This is the purpose of Fig. 6. Examination of this figure demonstrates the differences between the various experimental results. While at first glance such deviations may seem alarming, examination of the experiments themselves reveals the reason for the variations. Basically, Ghoshal's curves were determined on a relative basis and made absolute by comparison to a $Ni^{60}(\alpha,2n)Zn^{62}$ absolute measurement. Thus, the fact that his curves are somewhat higher than the present results is not particularly alarming. Furthermore, the shapes of Ghoshal's curves and the present curves are remarkably similar.

On the other hand, Meadows determined his cross sections by degrading 100 MeV protons and employing a beam monitor foil to measure the proton intensity. It is reasonable to suspect that his energy scale may therefore be somewhat inaccurate by comparison with experiments in which intensity is measured directly and the beam is degraded from "only" 30 MeV. Such appears to be the case, as Meadows' curves are considerably more broad than either Ghoshal's curves or the present results. In absolute magnitude, however, the present work is very close to that of Meadows. Thus the present experimental curves are essentially in agreement with the "strong points" of the work of previous experimenters even while disagreeing in overall appearance. Since these curves will be compared to results from the three other reactions to be discussed, it is essential that they be determined on the same basis. This has been accomplished by repeating these experiments. Moreover, it is felt that the present combination of previous results at specific energies with the newly determined absolute values for the cross sections of interest over the entire 5 to 30 MeV energy region is quite a good representation of the true excitation functions.

Examination of the experimental curves reveal very little that was not noticed by Ghoshal in his original work. The overall shape of these curves is typical of compound nucleus mechanisms. The high energy tail

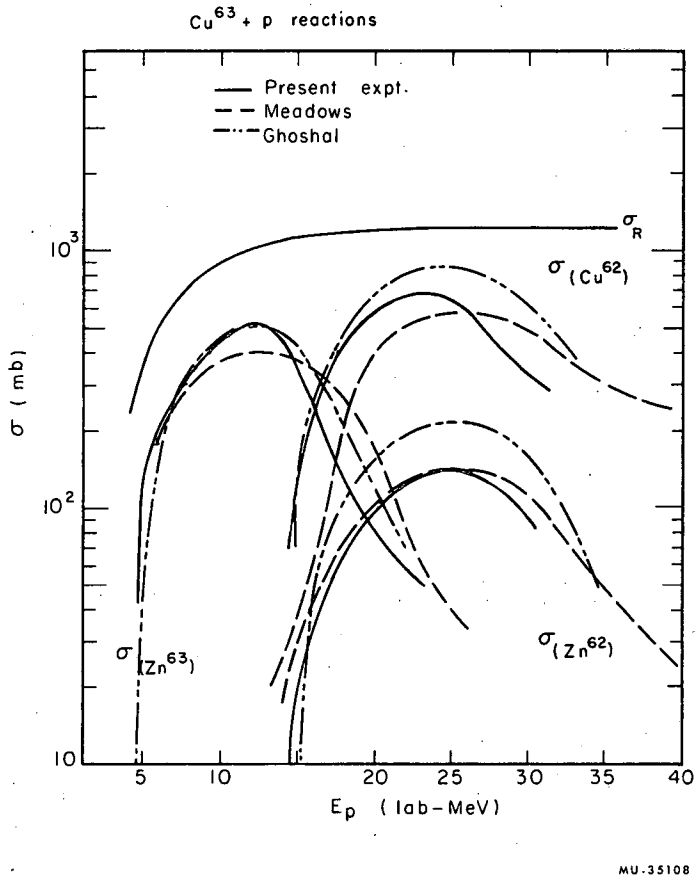

Fig. 6. Collection of available data for the p + Cu^{63} reactions, including the curves of Fig. 5, the results of Ghoshal (ref. 10), and the results of Meadows (ref. 11).

of the (p,n) curve is possibly due to a surface interaction of the "knock-out type." This is a predominant mechanism at higher energies than used here and might be expected to make a minor contribution to the observed cross section in this energy range. Howe[14] has invoked this mechanism as a possible explanation for his results with Cu^{63} + p reactions at energies barely above the Coulomb barrier. The high energy tail in the (p,pn) curve is probably due to inelastic scattering of the incident proton followed by neutron evaporation. Such a mechanism has been invoked by Reuland, Ganguly, and Caretto[47] to explain their recoil-range results for the $Cu^{65}(p,pn)Cu^{64}$ reaction.

The results are presented here without correction for other reactions which yield the same product. Since natural copper is bi-isotopic (69.1% Cu^{63} and 30.9% Cu^{65}), no such complications are expected. They would have to be, for example, the $Cu^{63}(p,n)$ + $Cu^{65}(p,3n)$ or $Cu^{63}(p,pn)$ + $Cu^{65}(p,p3n)$ and energy considerations are enough to rule out appreciable contributions from three or four particle evaporation. This reasoning is supported when the work of Meadows[11] for Cu^{65} + p is compared to the present experimental results.

2. $He^4 + Ni^{60}$

As one of the systems originally investigated by Ghoshal[10] these reactions are of particular interest for the present work. The results of Tanaka[12] are in disagreement with some of the previous determinations. The rather large difference between the results of these two experimenters is significant, and to resolve this difference these measurements were repeated. Cross sections measured during this series of experiments, Fig. 7, were quite similar to those found by Tanaka, and it would appear that Ghoshal's curves are of too great a magnitude and slightly shifted in energy as compared to the consensus of more recent work. This relationship is illustrated by Fig. 8. Low energy measurements of the $Ni^{60}(\alpha,n)Zn^{63}$ cross sections by McGowan, Stelson and Smith[13] agree well with the present results.

Since natural nickel was used as the target material, reactions with isotopes other than Ni^{60} are expected to contribute to the experimental

excitation functions. The nickel isotope present in largest abundance is Ni^{58} (~ 68%). However, only the $Ni^{58}(\alpha,\gamma)Zn^{62}$ reaction produces a possible interference, and the cross section for this reaction is quite small in the energy region where the $Ni^{60}(\alpha,2n)Zn^{62}$ reaction is measured. Also of concern would be reactions involving two or three particle emission from the compound nucleus Zn^{65} formed by $Ni^{61} + He^{4}$. In addition to the low cross sections for these reactions in the energy region of interest, the low isotopic abundance (~ 1%) does not permit interferences from reactions with Ni^{61}. Reactions with heavier isotopes of Ni may be ignored for the same reason. Therefore, no corrections for competing reactions have been applied to the data presented here.

The shapes of these curves are typical of compound nucleus reactions with a possible admixture of some non-compound mechanism appearing in the high energy tails. Such behavior is especially apparent in the curve for $Ni^{60}(\alpha,n)Zn^{63}$ as shown in Fig. 7. This effect appears to account for a sizable portion of the total cross section for this reaction, but does not appear to appreciably affect the shape near the peak in the curve. Excitation functions for the other reactions being considered are affected to a much smaller extent by non-compound processes contributing to the total cross sections. Such behavior is not unexpected because the probability for two particle stripping or two particle (non-compound) evaporation is probably not large for energies near the peak of the excitation function. As the energy is increased, however, such mechanisms become the most probable means of producing these nuclei, because a compound nucleus would have to boil off extremely high energy particles. Unfortunately, these curves do not reach high enough energies for this phenomenon to become obvious.

The relative magnitudes of the (α,pn) and $(\alpha,2n)$ excitation functions are of interest here. In spite of the supression of proton emission, by the Coulomb barrier, the cross section for the (α,pn) reaction is considerably greater than the cross section for the $(\alpha,2n)$ reaction. The greater probability for proton emission is explained by the greater number of available levels in the Cu^{62}(odd-odd) nucleus as compared to the corresponding number in the Zn^{62}(even-even) nucleus. Therefore there are more

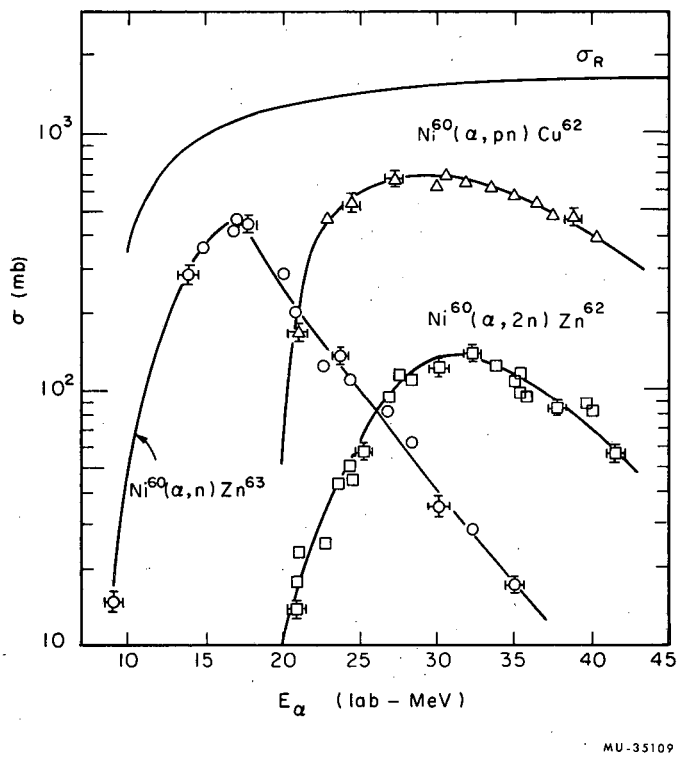

Fig. 7. Experimental excitation functions for He^4 + Ni^{60} reactions, including the total reaction cross section.

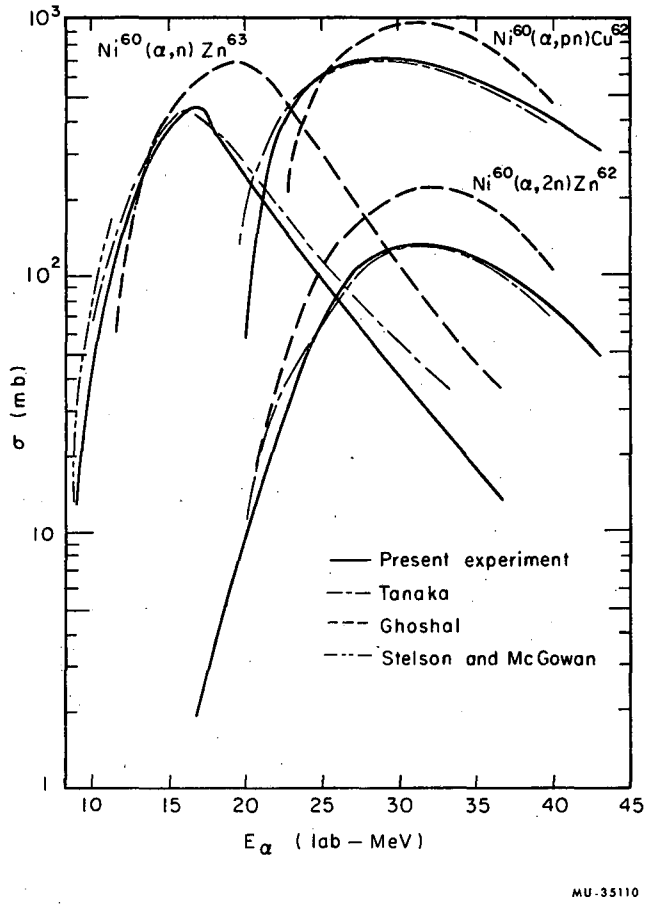

Fig. 8. Collection of available data for the He^4 + Ni^{60} reactions, including the curves of Fig. 7, and the results of Tanaka (ref. 12) Ghoshal (ref. 10) and McGowan, Stelson, and Smith (ref. 13).

open channels for the proton than for the neutron, and the cross section for proton emission is enhanced. The same phenomenon has been observed, by Markowitz, Miller, and Friedlander[48] in reactions of alpha particles with Cr^{50}, and was mentioned by Ghoshal in his original investigation of the present system. The enhancement of the proton emission probability is not only a property of the alpha particle system, but is also observed in all the systems that are included in this work.

3. $He^3 + Ni^{61}$

Excitation functions for He^3 reactions are of primary importance for this work because the same $[Zn^{64}]^*$ intermediate is involved here as is involved in Ghoshal's original experiments. However, the He^3 nucleus is also becoming increasingly important as a projectile for the study of a wide variety of reactions. Because of its low binding energy it is capable of inducing high states of excitation in the compound nucleus at relatively low incident (kinetic) energies. For this reason, He^3 reactions in the medium mass region, involving one particle boil-off only, are often limited by the Coulomb barrier. Such is the case for the $Ni^{61}(He^3,n)Zn^{63}$ reaction in this study (Fig. 9). Only the high energy side of the excitation function appears above the Coulomb barrier. As will be seen presently, this high energy tail may be partially due to contributions to the $Ni^{61}(He^3,n)Zn^{63}$ excitation function from the $Ni^{62}(He^3,2n)Zn^{63}$ reaction. However, such interference probably accounts for only 20% of this tail at the most. The presence of the observed $Ni^{61}(He^3,n)Zn^{63}$ excitation function in this energy region is worth further consideration.

Reactions involving alpha particle emission and three particle emission are energetically possible near the Coulomb barrier for He^3 and Ni^{61}. Furthermore, the Q value for the reaction $Ni^{61}(He^3,n)Zn^{63}$ is positive (+ 4.8 MeV), indicating that the reaction threshold is, in effect, the Coulomb barrier. Therefore, by statistical considerations the contributions of one particle emission to the total reaction cross section should have peaked and become quite small, even at the lowest experimentally accessible energies. The fact that it is not small indicates the possible

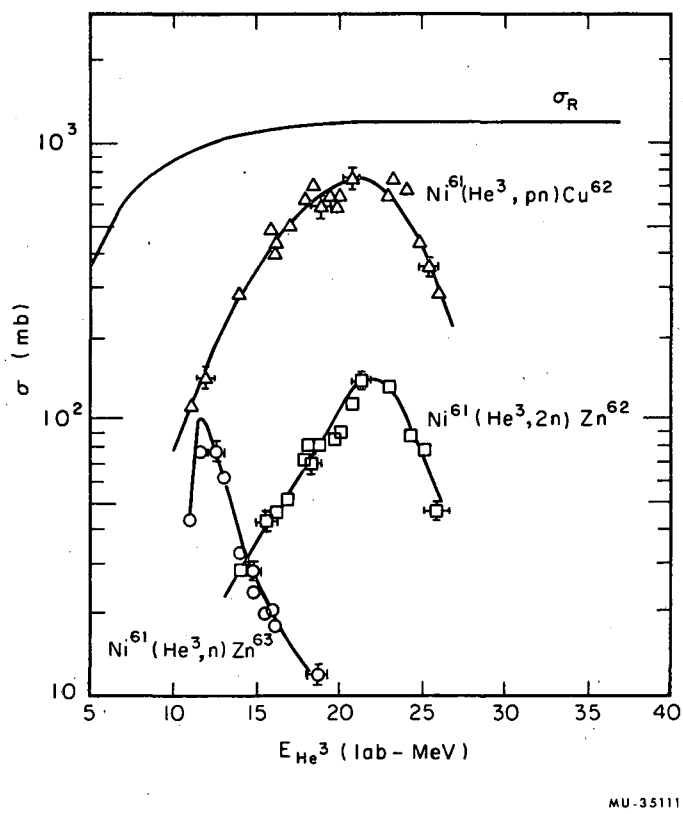

Fig. 9. Experimental excitation functions for the He^3 + Ni^{61} reactions, including the total reaction cross section.

presence of non-compound reaction mechanisms. The very fact that the He^3 nucleus is loosely bound would lead us to suspect that mechanisms involving direct interaction might be of importance in its reactions. Presumably these would be two particle stripping or a local hot spot boil-off of the neutron before thermal equilibrium could be achieved. It is not possible to select one of these mechanisms, or any other, as being responsible for the observed tail on the basis of these experimentations.

Examination of the excitation functions for the $Ni^{61}(He^3,2n)Zn^{62}$ and $Ni^{61}(He^3,np)Cu^{62}$ reactions reveals the presence of very slight high energy tails on a compound nuclear appearing peak. Both these reactions are energetically possible at the Coulomb barrier and rise rapidly to a peak at 21.5 MeV, about 10 MeV above the barrier. The decline in cross section as the energy is further increased proceeds more slowly. This behavior is typical of He^3 reactions in the medium mass region. Comparison of these curves with, for example, the results of Bryant, Cochran and Knight[49] for He^3 reactions with copper nuclei serves to illustrate this trend.

Since the enriched Ni^{61} target material contains substantial amounts of other nickel isotopes (Table I) their contributions to the experimental excitation functions must be evaluated. Nickel-58 cannot interfere in these reactions. Presumably the high energy tail for the $Ni^{60}(He^3,n)Zn^{62}$ could contribute to the cross section measured for the $Ni^{61}(He^3,2n)Zn^{62}$ reaction. It is unlikely that this contribution is large enough to cause concern, because Ni^{60} is a factor of 10 less abundant than Ni^{61} in the target material. Furthermore, the $Ni^{60}(He^3,n)Zn^{62}$ reaction cross section in this energy region is expected to be quite small ($\simeq$ 10 millibarns) by analogy to similar reactions on copper isotopes[49] and the present results for Ni^{61}, as well as from energy considerations.

Contributions to the $Ni^{61}(He^3,2n)Zn^{62}$ and $Ni^{61}(He^3,pn)Cu^{62}$ reactions are expected from the corresponding $(He^3,3n)$ and $(He^3, 2np)$ reactions on Ni^{62}. By analogy to the copper measurements the two cross sections are of the same order of magnitude at energies somewhat higher than the peak in the curve for two particle boil off. Fortunately, there is only about

1/20th of this contribution in the present data due to relative isotopic abundances in the target. Therefore, contributions from Ni^{62} reactions will not significantly affect the Ni^{61} excitation functions except at energies well above the peaks and out of the energy range being studied. Production of Zn^{62} from $Ni^{61} + He^{3}$ is, at these energies, expected to be nearly all by a compound nuclear mechanism, since non-compound reactions would have to be quite complex to effect this transformation. Therefore, the fact that the experimental curves for this reaction show no significant high energy asymmetry justifies the neglect of Ni^{62} reaction contributions in the presentation of these results. A fortiori contributions from Ni^{64} reactions can be ignored.

This lack of complications from reactions involving isotopes of nickel other than Ni^{61} implies that any high energy tail observed on the excitation function for $Ni^{61}(He^{3},pn)Cu^{62}$ is due to a non-compound nuclear mechanism. Since production of Cu^{62} may be affected by transfer of a single proton from the He^{3} nucleus, it is surprising that the experimental data presents only slight evidence for competition between compound and direct processes in the present energy region.

4. $C^{12} + Cr^{52}$

Heavy ion reactions are generally conceded to proceed through formation of a compound nucleus unless the products are of a mass near that of the target. See for example the results obtained by the Yale group.[50,51] For products of mass near the target mass there is simply not enough energy in a hypothetical compound system to boil off enough particles. Conversely, for products of mass nearer the combined target and projectile mass the complexity of a mechanism allowing transfer of a large number of nucleons without compound nucleus formation is prohibitive. The appearance of high energy tails on the experimental excitation functions (Fig. 10) is, therefore, probably not due to non-compound reaction mechanisms.

The high energy asymmetry that appears on these excitation functions may be attributed to contributions from the $Cr^{53}(C^{12},3n)Zn^{62}$ and $Cr^{53}(C^{12},p2n)Cu^{62}$ reactions. Cross sections for these reactions would be

expected to be on the order of 100 millibarns by comparison with other such reactions in the medium mass region.[50,52] Since the isotopic ratio of Cr^{52} to Cr^{53} is ten, we would expect about 10 millibarns contribution to the measured Cr^{52} cross sections from reactions involving Cr^{53} at the peak in its excitation function, with less contribution at lower energies. This peak will appear at roughly 60-70 MeV judging by the trend in the present data. Therefore, the measured excitation functions extending to 65 MeV will be influenced by Cr^{53} reactions to the extent of 5 to 10 millibarns. Examination of the experimental curves suggests that this estimate is essentially correct. However, due to the dubious quantitative accuracy of the above argument no attempt has been made to correct the experimental results for the presence of Cr^{53} reactions.

Energy considerations and a factor of 40 in isotopic abundance preclude the possibility of contributions from Cr^{54} reactions to the measured excitation functions.

As was the case with the (He^3,n) reaction on Ni^{61}, the (C^{12},n) reaction is supressed by the Coulomb barrier. Attempts were made to detect the presence of Zn^{63} in the reaction products at energies near the barrier but very little, if any, was found. This low cross section at experimentally attainable energies implies that contributions from the $Cr^{53}(C^{12},2n)Zn^{63}$ reaction are small in this region, and also that non-compound processes with their "high" energy tails are not operative. In view of the foregoing discussion neither of these observations is unexpected.

B. Forward Scattering and Range Measurements for Zn^{62} Recoils

In the preceding section, the conclusion was reached that formation of Zn^{62} proceeds almost exclusively through a compound nuclear reaction mechanism for the systems under investigation. The shape of the experimental excitation functions is not always a sufficient criterion for determining reaction mechanisms. For this reason several experiments were performed to compare experimental range measurements with ranges calculated assuming a compound nucleus mechanism. Comparisons of this

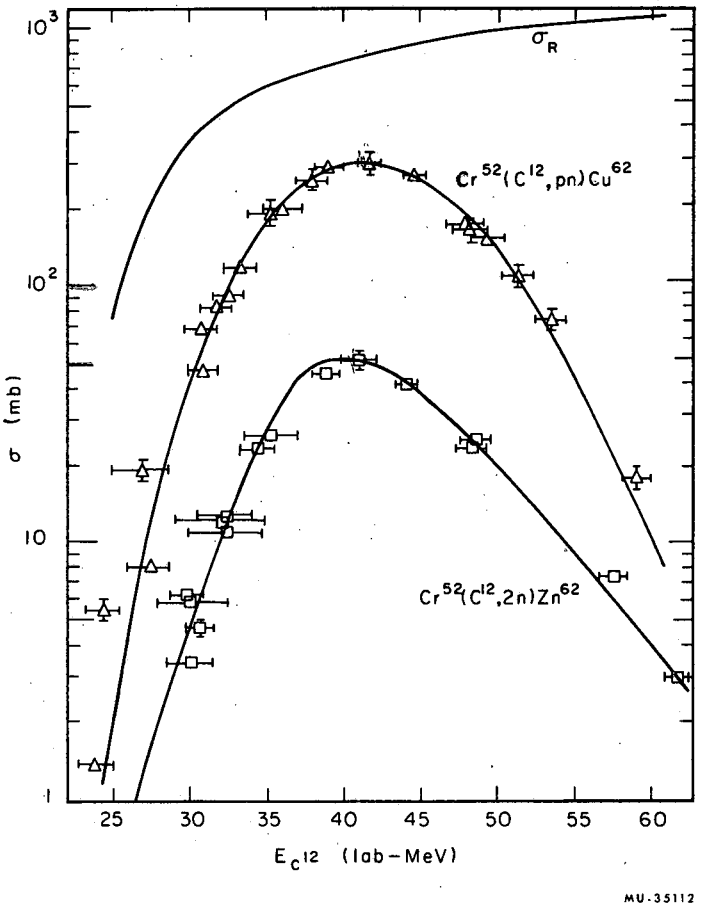

Fig. 10. Experimental excitation functions for the C^{12} + Cr^{52} reactions, including the total reaction cross section.

type are of value because only in complete particle-target fusion reactions will the recoils have an energy distribution about the maximum energy allowable from conservation of momentum. Reactions proceeding by other mechanisms will produce recoils having a rather large energy distribution. Emission of individual nucleons during the decay of the compound system affects the velocity of the recoil only slightly due to the large mass differential of the two fragments. The assumption that, on the average, the decay processes do not alter the velocity of the recoil permits its energy to be expressed in terms of Eq. 4.

Associated with the energy of a fragment is a mean range in a given material. Due particularly to range straggling, a rather broad distribution of total path lengths is an inherent property of the system. This distribution is generally assumed to be Gaussian in shape. Lindhard, Scharff and Schiøtt[39] have developed the theory of range-energy relations to the extent that theoretical predictions of recoil ranges can be made and compared to experimentally determined ranges. Such comparisons often are used to provide insight into the reaction mechanisms.[53-56] The calculational procedure has been described in Sec. II-C, while the curves relating the average of the projected range distribution to recoil energy are shown in Fig. 4.

Experimental range measurements are not always necessary to check the compound nuclear nature of a reaction. Simply by comparing experimental and theoretical forward and backward scattered recoil fractions it is generally possible to establish the amount of momentum transfer, and thereby the general type of reaction. If it is possible, as in the present case, to neglect the change in velocity of the recoil fragment accompanying emission of decay particles, then the backward scattering fraction is very nearly zero and may also be neglected. It can also be shown that the forward fraction (F) is essentially unity for a recoil with a projected range ($\overline{R}_p$) greater than the target thickness (W) and is given for the case $\overline{R}_p \leq W$ by[57]:

$$F = \frac{R_p}{W} \qquad (5)$$

During the course of this research, four recoil experiments were performed. Two of these were of the thick target type ($\overline{R}_p < W$), while the other two used a thin target ($\overline{R}_p \gg W$). All were concerned with Zn^{62} recoils having a recoil energy between 1.2 and 2.2 MeV. The results are presented in Table 5.

For the experiments in which $\overline{R}_p < W$ (numbers 1 and 2) the quantity $\overline{R}_p$ could not be measured. A continuous distribution in the ranges of the recoils escaping from the target was observed, and was attributable to energy loss and/or scattering occurring in the target. The excellent agreement between experimental and theoretical forward scattering fractions is perhaps a bit fortuitous, but serves to demonstrate the complete momentum transfer that is characteristic of compound nuclear reactions.

Forward scattering fractions are of no value in the third and fourth experiments listed in Table V because in this case $R \gg W$ and F must, therefore, be nearly unity. For these experiments a series of aluminum leaf catcher foils (0.75 mg/cm^2) were placed downbeam from the target foil. Figure 11 shows a typical, raw range distribution according to foil number. The fraction of the total activity (F_t) passing through each foil was plotted against total thickness (t) on probability paper, as in Fig. 12. A straight line could easily pass through the points indicating that the range distribution was essentially Gaussian. The thickness through which 50% of the recoils passed can be read from the graph and represents the peak in the distribution. This thickness is the experimental value of the mean projected range, $\overline{R}_p$, and is to be compared with the value for a compound nuclear reaction calculated according to Lindhard et al. From Table 5 it is easily seen that the two values are in quite good agreement.

The results of these experiments lend strong support to the notion that Zn^{62} is produced through compound nuclear reactions by the reactions here investigated. However, if one is willing to accept the idea that these reactions are known to be compound nuclear from previous data, then the results presented here lend strong support to the calculational procedures used in computing the range values. Perhaps the latter consideration will prove to be the more valuable of the two. With this in mind,

Table V. Results of recoil range experiments.

1. $He^3 + Ni^{61}$	$E_B = 24.3$ MeV $W = 1.55$ mg/cm^2 $E_R = 1.14$ MeV $\bar{R}_p = 0.16$ mgAl/cm^2	$F_{expt} = 0.098$	$F_{th} = \frac{\bar{R}_p}{W} = 0.12$	$\bar{R}_{p(expt)}$ - not measured
2. $He^4 + Ni^{61}$	$E_B = 35.3$ MeV $W = 2.35$ mg/cm^2 $E_R = 2.2$ MeV $\bar{R}_p = 0.32$ mgAl/cm^2	$F_{expt} = 0.13$	$F_{th} = 0.13$	$\bar{R}_{expt}$ - not measured
3. $He^4 + Ni^{61}$	$E_B = 35.3$ MeV $W = 0.044$ mg/cm^2 $E_R = 2.21$ MeV $\bar{R}_p = 0.32$ mgAl/cm^2	$F_{expt} = 1$	$F_{th} = 1$	$\bar{R}_{p(expt)} = 0.28$
4. $He^4 + Ni^{61}$	$E_B = 32$ MeV $W = 0.044$ mg/cm^2 $E_R = 2.0$ MeV $\bar{R}_p = 0.31$ mgAl/cm^2	$F_{expt} = 1$	$F_{th} = 1$	$\bar{R}_{p(expt)} = 0.34$

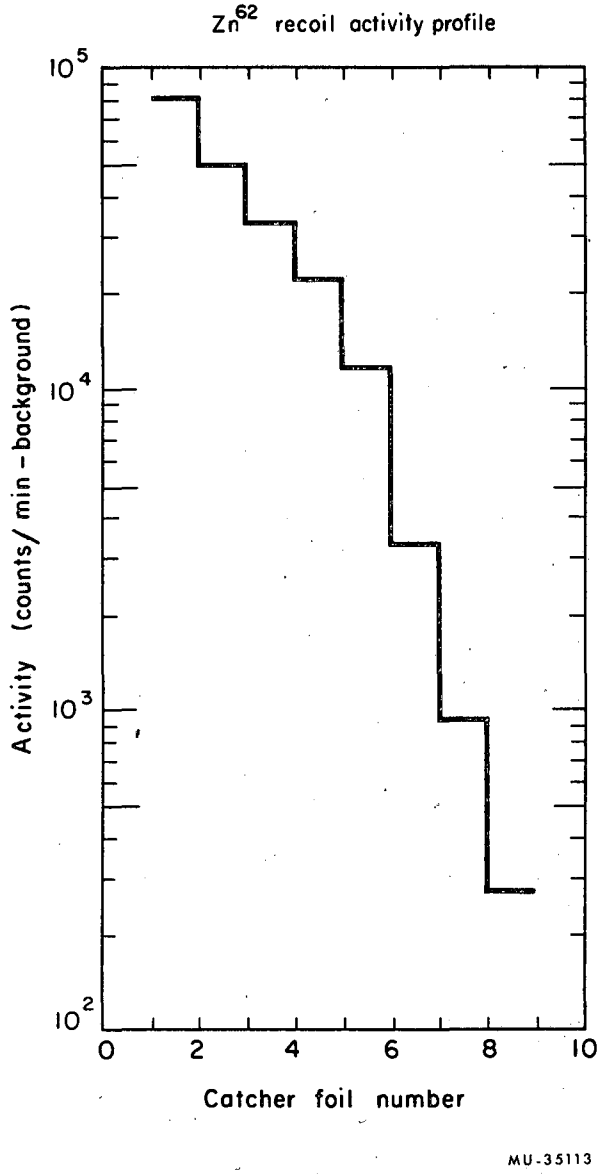

Fig. 11. Activity distribution of Zn^{62} in catcher foils for a typical recoil-range experiment.

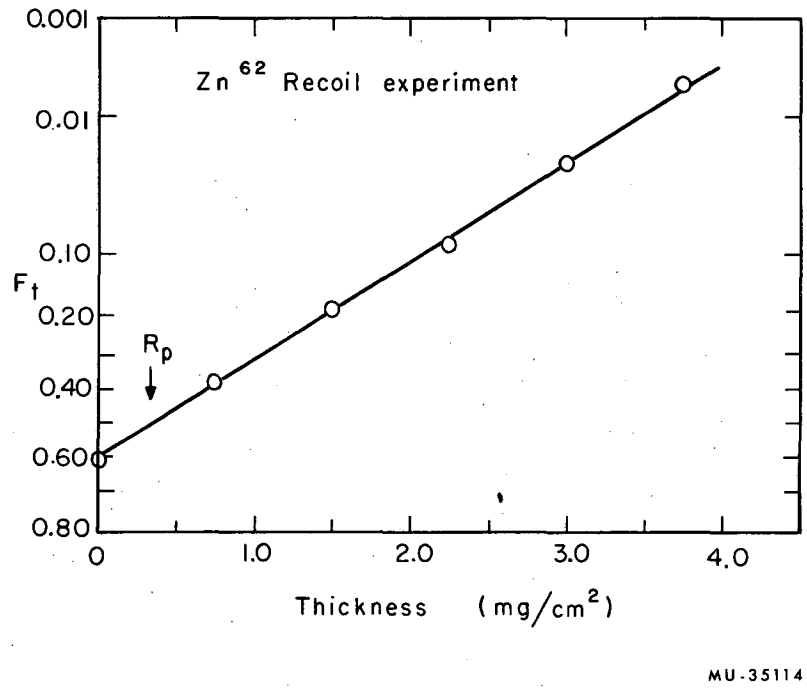

Fig. 12. Activity profile of the data from Fig. 11 plotted on a probability scale. F_t is the fraction of the total recoils passing through a thickness, t.

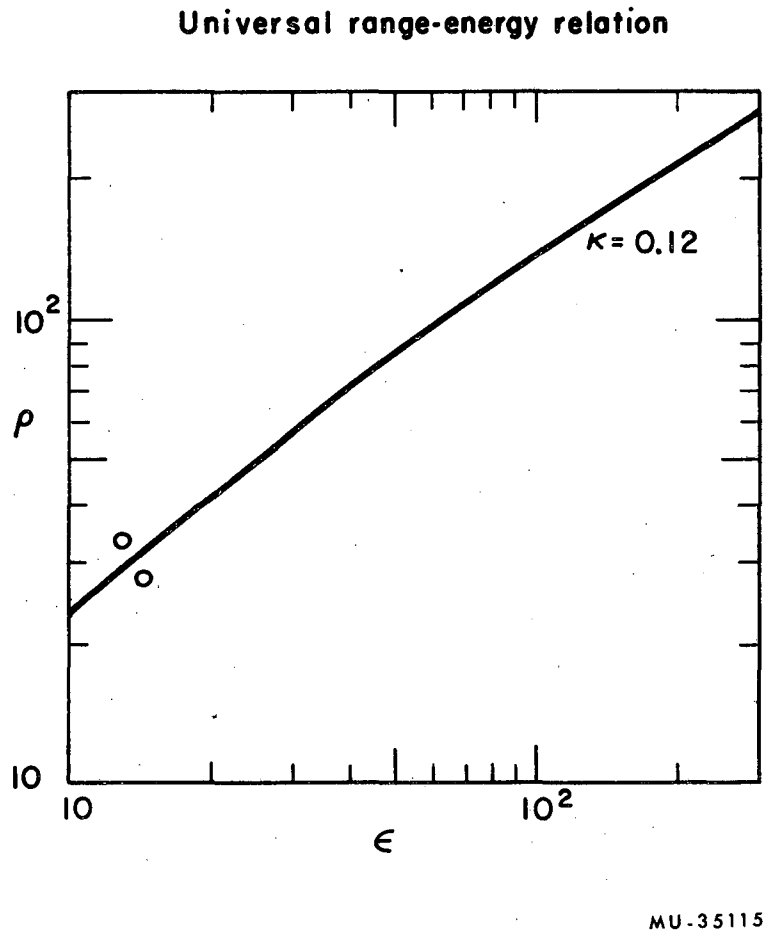

Fig. 13. Universal range energy curve showing the experimental results for Zn^{62} recoils. (ρ, ϵ and κ are the dimensionless range, energy and electronic stopping parameters described in ref. 39).

a universal range-energy (ρ vs ϵ) plot for the appropriate electronic stopping parameter (κ) is presented in Fig. 13 including the experimental values obtained.

For the present purposes, however, we shall adopt the former interpretation, taking these results as evidence for a compound nucleus mechanism. Similar experiments involving Zn^{63} and Cu^{62} recoils would help define the overall reaction mechanism beyond reasonable doubt. Measuring ranges for these materials, however, will be left to the discretion of some future experimenter.

C. Estimation of Errors

1. Errors in Absolute Cross Sections

The uncertainty in defining the energy at which a given cross section is measured is due primarily to the energy spread in the projectile beam. This amounts to ± 2% at the first foil and increases to ± 5% for the last target foil in the stack. Finite target thickness is a factor and accounts for an energy range which varies in magnitude from 1% to ± 6% depending on the details of the target-beam-energy system. Thus, overall uncertainty in the energy scales is ± 1% for p, ± 3% for He^4, ± 2% for He^3, and ± 6% for C^{12} bombardments in the average case.

Uncertainty in cross section measurements is taken as roughly equal to the uncertainty in determination of the activity extrapolated to time zero. This error is dependent primarily on the complexity of the decay curve (i.e., the number of subtractions needed to obtain the points defining the decay of the nuclide of interest). Such uncertainties have been estimated at ± 2-3% for the first or longest-lived component to ± 6-10% for the fifth component. These errors are assigned to each determination individually.

A detailed summary of the sources of error, their magnitude, and their contribution to the overall uncertainties listed above is given in Appendix VI.

2. Errors in Recoil-Range Experiments

The essential experimental quantity for these calculations is the time zero intercept of the activity due to the Zn^{62} produced during the

reaction. This determination, by decay curve analysis, introduces an uncertainty of 3-4%. Furthermore, where the recoil range is under investigation (as opposed to forward scattering fraction) the thickness of the catcher foils is a second source of error. In this work the aluminum catcher foils were 0.75 ± .015 mg/cm^2 thick and introduced another 2% error. For thick target experiments the target thickness is an important quantity. It is felt that this value is known to ± 2%. According to these estimates, the experimental ranges or forward scattering fractions are known to within 5%.

IV. THEORETICAL CONSIDERATIONS APPLIED TO THE EXPERIMENTAL RESULTS

In this section, predictions of various classical theories will be compared to the experimental results. As one of the primary goals of this research was to provide an extreme test of the independence postulate, this subject will be treated in rather great detail. The effects of angular momentum upon the behavior of the compound system, as they apply to compound nuclear theory will, of necessity, be discussed. Finally, it will be seen whether or not statistical theory, in its present form, can be invoked to aid our understanding of the significance of these experiments.

A. Comparison of Excitation Functions

For the interaction between a bombarding particle, a, with a target nucleus, A, compound nuclear theory predicts the formation of an excited intermediate system, C*, which subsequently decays along one of several available exit channels, W.

$$a + A \longrightarrow C^* \longrightarrow w + W \qquad (6)$$

The actual mode of decay, or exit channel, is determined by statistical considerations according to the energy of excitation, binding energy, particle spins, conservation laws, etc., and is usually represented by P_w, the probability that C* will decay through the channel w. Similarly, the probability of forming the compound system is the overall reaction cross section, σ_R. We can, therefore, write the cross section for formation of the products (w + W) as

$$\sigma_w = \sigma_R P_w (C^*) \qquad (7)$$

This is a mathematical expression of the independence postulate, and as such demonstrates the two part nature of this model of nuclear reaction mechanisms. One of the primary goals of this work is to provide an extensive test of the independence concept.

It is of interest to develop the theory to include several entrance channels, u, as well as several exit channels, w. For each u there will be an equation similar to Eq. 7:

$$\sigma_{u,w} = \sigma_R(u)\, P_w(C^*) \tag{8}$$

Noting that $P_w(C^*)$ is a function only of the properties of the compound system, it is observed that

$$\frac{\sigma_{(u,w)}}{\sigma_R(u)} = \text{constant} \tag{9}$$

for production of identical C*'s through several channels, u. In the present work we are considering the reactions:

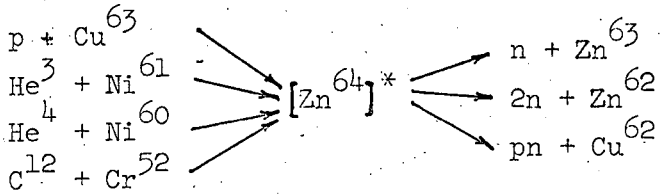

If compound nuclear theory completely describes these interactions then, from Eq. 8 we would expect

$$\frac{\sigma_{(p,w)}}{\sigma_R(p)} = \frac{\sigma_{(He^3,w)}}{\sigma_R(He^3)} = \frac{\sigma_{(He^4,w)}}{\sigma_R(He^4)} = \frac{\sigma_{(C^{12},w)}}{\sigma_R(C^{12})} \tag{10}$$

for each of the three exit channels, w, that were experimentally observed.

Before this classical test of the theory may be made, it is necessary to develop two further concepts. In the first place, a good, self-consistent set of total reaction cross sections is required. This problem is discussed in the next section. Secondly, a comparison such as that indicated in Eq. 10 is valid only if the ratios are taken from results derived from identical compound nuclei. In other words, the experimental curves must be adjusted along the energy axis to compensate for differences

in the compound nuclei. Traditionally this adjustment is accomplished by transforming the laboratory energy to a quantity referred to as the excitation energy and involves corrections for conservation of momentum and projectile-target binding energy differences. This energy transformation is the subject of the second section following.

With these concepts, the comparison indicated in Eq. 10 will be made and the implications of the results examined.

1. Total Reaction Cross Sections

If the probability of forming the compound nucleus (σ_R) is taken as the total reaction cross section it becomes possible to calculate this quantity by using the optical model of nuclear reactions. The computer program OPTIC,[58] written for the purpose of calculating inelastic scattering cross sections, was adopted for this purpose. The optical model potential may be written as

$$V(r) = V_c(r) + Uf(r) + iWg(r) + (U_s + iW_s)\frac{1}{r}\frac{df(r)}{df} l \cdot \sigma \qquad (11)$$

where $V_c(r)$ = Coulomb potential $\begin{cases} = \dfrac{ZZ'e^2}{r} & r \geq R \\ = \dfrac{ZZ'e^2}{2R}\left[3 - (r^2/R^2)\right] & r < R \end{cases}$

U = real potential depth

W = imaginary potential depth

U_s and W_s = real and imaginary spin orbit potentials

l = orbital angular momentum

σ = Pauli spin operator

r = radial distance between centers of interacting bodies

R = radius of target = $r_0 A_T^{1/3}$

$f(r)$ = Saxon-Woods form factor = $\dfrac{1}{1 + \exp\{(r - R)/a\}}$

$g(r)$ = surface Gaussian form factor = $\exp\{-(r - \frac{R}{b})^2\}$

a and b = diffuseness of the real and imaginary potential surfaces.

For the present purpose the optimum potential suggestions of Hodgson[59] were generally adopted. Accordingly, the spin-orbit term was not used and the form factors were set equal to each other, following the Saxon-Woods configuration. Furthermore, since scattering was not of primary concern the diffuseness parameters of the real and imaginary potentials were chosen equal. Of primary importance in optical model calculations is the interaction radius, usually written as

$$R_{int} = r_0 A_T^{1/3} + r_1 \qquad (12)$$

For general convenience Hodgson recommends that r_1 be taken as zero, and that r_0 be varied to account for its absence. However, as the results from OPTIC calculations are to be used later in development of the effects of angular momentum, it is desirable to select a particular radius constant and to include an r, additive term such that the interaction radii used corresponded to those recommended. Choosing $r_0 = 1.25$ Fermis the interaction radius

$$R_{int} = r_0(A_T^{1/3} + A_u^{1/3}) \qquad (13)$$

is quite near the values calculated from Hodgson's variable r_0's. Thus the input parameter r_1 is simply

$$r_1 = 1.25 A_u^{1/3} \qquad (14)$$

The input parameters for the OPTIC calculations that were used to obtain the total reaction cross sections are presented in Table VI. These parameters are those of Hodgson for the proton and Helium-3 calculations. The variation of potentials with energy closely predicts experimental "best fit" potentials for p + Cu[63] where they involve roughly the same radial and diffuseness parameters adopted here.[60] The same is true for the He^3 reaction.[61] Parameters chosen for the alpha particle calculations, while being very near those suggested by Hodgson, are the "best fit" values of Bassel et al.[62] No suggestions or experimental values are available for

Table VI. Parameters for optical model calculations.

Reaction	E range (MeV)	V_R (MeV)	V_I (MeV)	a,b	r_0	r_1
$p + Cu^{63}$	5-35	58-0.3 E	$3\ E^{1/2}$	0.65	1.25	0
$He^3 + Ni^{61}$	10-35	28.2	28.2	0.65	1.25	1.80
$He^4 + Ni^{60}$	10-50	47.6	13.8	0.60	1.25	1.98
$C^{12} + Cr^{52}$	20-60	50	15	0.60	1.25	2.86

carbon interacting with medium weight nuclei. Therefore, the parameters had to be chosen by inference from trends in the alpha particle potentials and from data collected on various nitrogen-light nuclei interactions by Bassel.[63] In general, while no claims can be made that the parameters chosen represent the best fit to scattering data at all energies, it is expected that the transmission coefficients and reaction cross sections obtained here are reasonably good over the entire energy range of interest and are quite good near the energies of available scattering experiments.

In the general case the total reaction cross section, $\sigma_R(J_c,E)$, may be written as

$$\sigma_R(J_c,E) = \pi\lambda\!\!\!^{-2} \sum_{S=|I-s|}^{|I+s|} \sum_{\ell=|J_c-S|}^{|J_c+S|} \frac{2J_c+1}{(2s+1)(2I+1)} T_\ell(E) \qquad (15)$$

where $\lambda\!\!\!^{-}$ = deBroglie wavelength of the incoming projectile/2π

I = spin of the target nucleus

s = spin of the projectile

$T_\ell(E)$ = transmission coefficient of a particle with orbital angular momentum (ℓ) and energy (E)

J_c = spin of compound nucleus.

For the cases where $I = s = 0$ (i.e., $He^4 + Ni^{60}$ and $C^{12} + Cr^{52}$) Eq. 15 reduces to $\pi\lambda\!\!\!^{-2}(2J_c+1)T_{J_c}(E)$

$$\sigma_R(J_c,E) = \pi\lambda\!\!\!^{-2} \sum_{J_c\ell}^{J_c} (2\ell+1)\, T_{\ell J_c} \qquad (16)$$

The OPTIC program includes the results of a calculation of Eq. 16 as part of its output. For the reactions involving non-zero spins ($He^3 + Ni^{61}$ and $p + Cu^{63}$) the transmission coefficients obtained from the OPTIC calculation were used as input for a calculation according to Eq. 15 by the ISOMER computer program.[64] The total reaction cross sections thus obtained are plotted, along with the experimental excitation functions in Figs. 5, 7, 9, and 10.

2. Excitation Energy

The comparison of excitation functions as indicated in Eq. 10 is predicted upon the assumption that the compound nuclei are identical. It is therefore necessary to adjust the energy scales for the various excitation functions to correspond to a common energy scale representing the energy of excitation possessed by the compound intermediate formed during the reaction. This excitation energy derives from the kinetic energy of the incoming projectile (less the compound nuclear recoil energy) and from the energy of binding the target and projectile to form the compound nucleus. Thus:

$$E^* = \left(1 - \frac{m_p}{m_c}\right) T_p + E_{BE} = \left(\frac{m_T}{m_c}\right) T_p + E_{BE} \qquad (17)$$

where E^* = excitation energy in the compound nucleus

m_p, m_T, m_c = mass of projectile, target, and compound nucleus, respectively

T_p = kinetic energy of the projectile (laboratory system)

E_{BE} = binding energy of the projectile to the compound nucleus ($E_{BE} = (m_p + m_T - m_c)\, c^2$).

The masses used to obtain excitation energies are those given (as mass defects) in the 1960 Nuclear Data Tables.[65] A graphical presentation of the relationship between laboratory energy of the projectile and excitation energy of the compound nucleus is given by Fig. 14. It is interesting to note in passing that, as seen from this graph, the low binding energy of the He^3 particle makes it extremely useful for obtaining high excitation energies at low bombarding energies as compared to the other projectiles used. Also of interest is the degree of excitation possible with the various projectiles at the Coulomb barrier. Figure 14 illustrates the similarity in this respect of the proton- and alpha particle-induced reactions. It also demonstrates that the Zn^{64} formed with either He^3 or C^{12} projectiles will have sufficient excitation energy, even at the Coulomb barrier, to boil off more than one particle, and explains the lack of appreciable cross section for the (He^3,n) and (C^{12},n) reactions described previously.

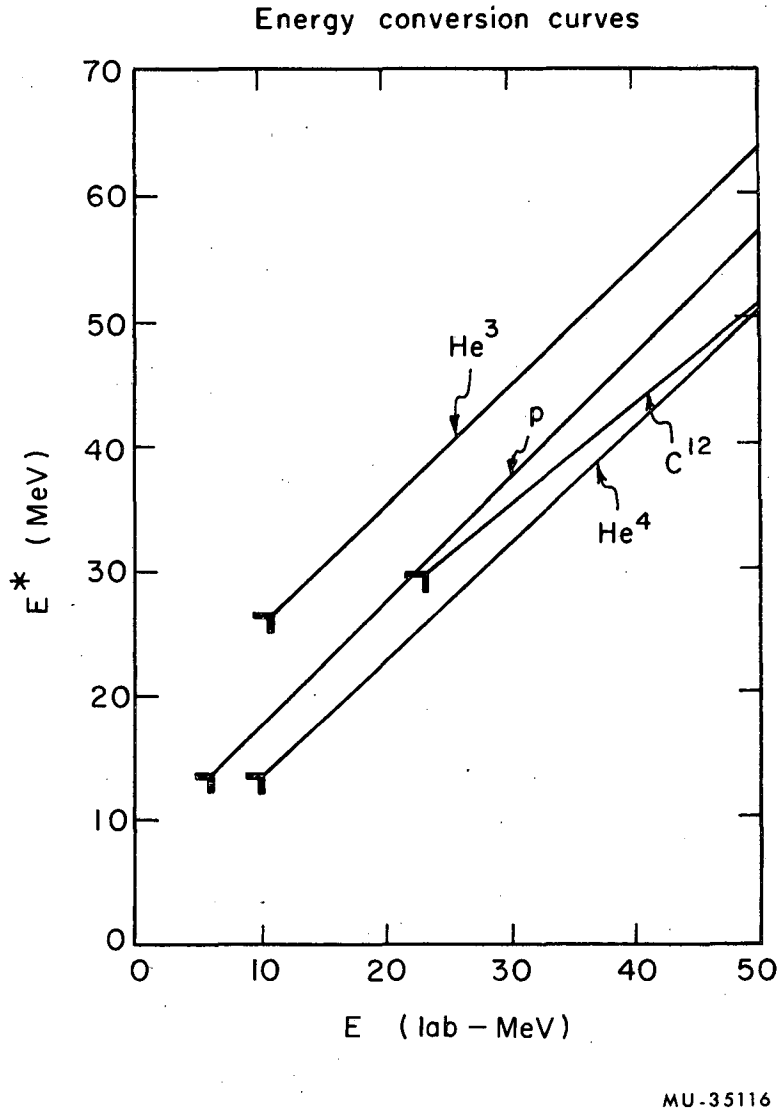

Fig. 14. The relationship between laboratory projectile energy and the corresponding excitation energy of the Zn^{64} compound nucleus. Coulomb barriers are indicated.

3. Classical Test of the Independence Postulate

In this section, the independence postulate is to be subjected to a test according to the dictates of Eq. 10. Accordingly, the laboratory projectile energies have been transformed to excitation energies by application of Eq. 17. Furthermore, the experimental cross sections have been reduced to fractions of the total reaction cross sections obtained from the OPTIC and ISOMER calculations based on Eq. 15. These ratios are plotted versus excitation energy in Figs. 15 to 17. By photo-excitation of Zn^{64}, the $[Zn^{64}]^*$ compound nucleus can be formed in various degrees of excitation. The results of these experiments, performed by Sagane,[66] are also included in Figs. 15, 16, and 17.

If all the curves in each figure coincided, then the requirements of Eq. 10 would have been satisfied. The fact that these curves do not agree indicates the failure of the independence postulate in its classical sense. If, however, we ignore the energy positions of the peaks for the time being, and simply compare the shapes of the curves, a remarkable degree of similarity is noticed. Not only is the shape similar, the overall fraction of the total reaction cross section is effectively constant for all entrance channels. These observations indicate that the failure of the classical theory may simply be due to the choice of energy scales used in the comparison. Clearly, the concept of excitation energy as defined in Eq. 17 does not accurately reflect the true state of the compound system.

Classically the energy of the compound system controls its decay. In the more modern sense of the independence postulate, it is recognized that if one is to compare similar systems, then corrections must be made in the energy scale for all factors that influence the choice of decay modes. One such factor, the most probable explanation for the failure of classical theory, is angular momentum. The effects of rotation upon the decay of the compound system are discussed in the next section, where also, an attempt to find an explanation for the discrepancy between the present experimental results and the theory will be made.

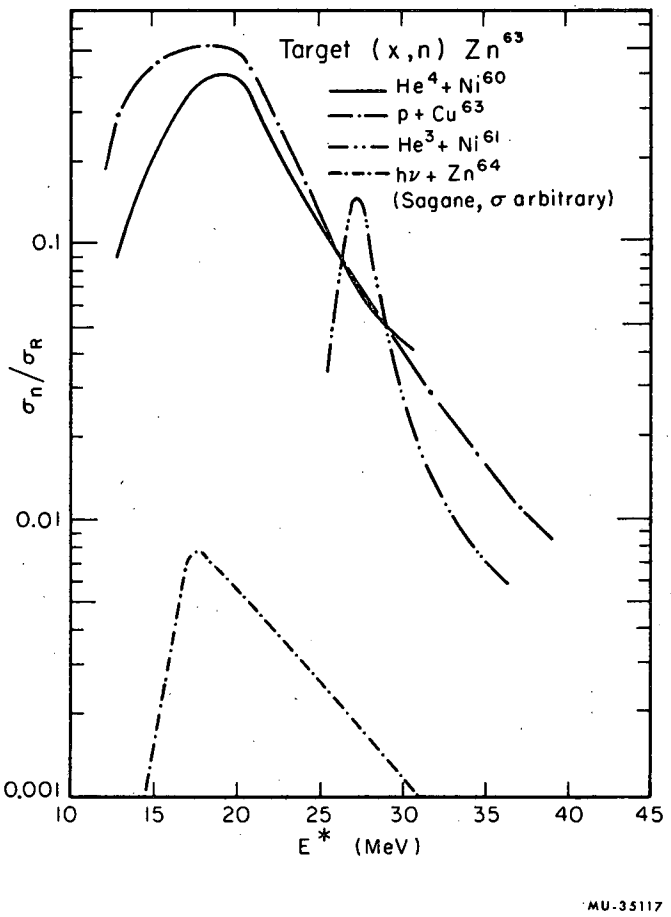

Fig. 15. The ratio of (x,n) cross sections to the total reaction cross section as a function of excitation energy of the compound system. The $Zn^{64}(h\nu,n)Zn^{63}$ excitation function of Sagane (ref. 66) is shown on an arbitrary cross section scale.

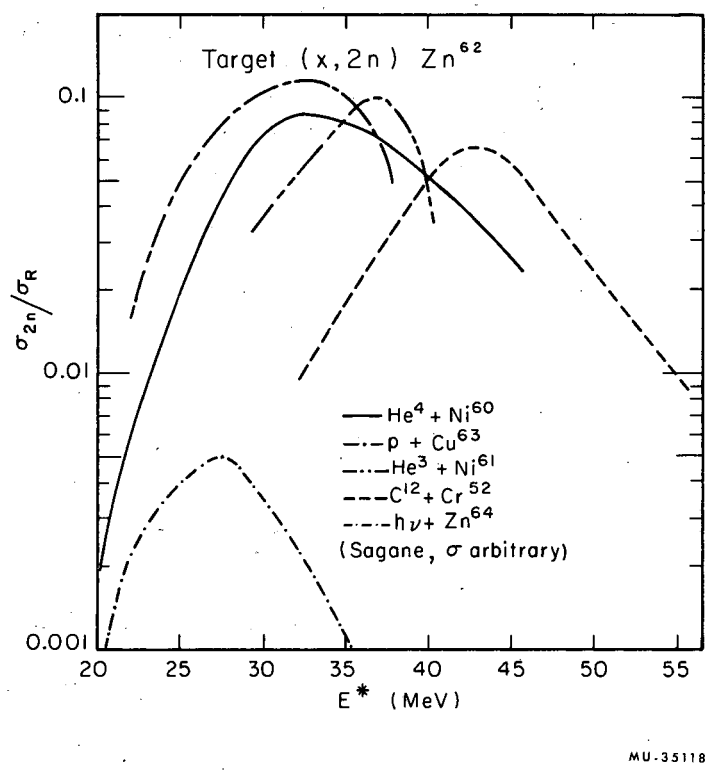

Fig. 16. The ratio of (x,2n) cross sections to the total reaction cross section as a function of excitation energy of the compound system. The $Zn^{64}(h\nu,2n)Zn^{62}$ excitation function of Sagane (Ref. 66) is shown on an arbitrary cross section scale.

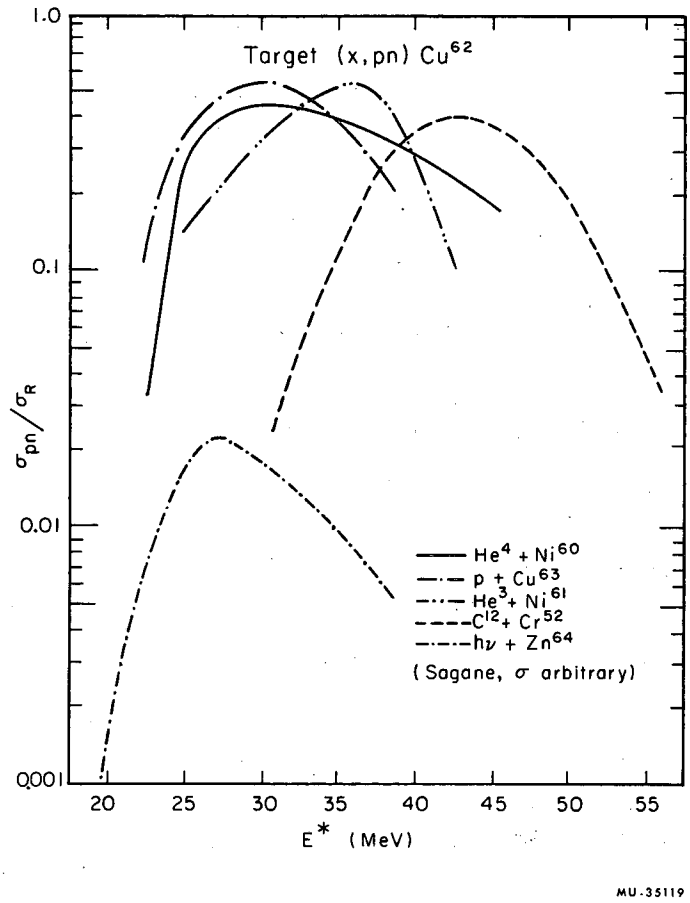

Fig. 17. The ratio of (x,pn) cross sections to the total reaction cross section as a function of excitation energy of the compound system. The $Zn^{64}(h\nu,pn)Cu^{62}$ excitation function of Sagane (ref. 66) is shown on an arbitrary cross section scale.

B. Angular Momentum Effects

In the past few years the effect of angular momentum on compound nuclear de-excitation has received increasing attention. Mollenauer[67] has shown that gamma ray emission, normally negligible, is successfully able to compete with neutron emission for reactions involving large amounts of angular momentum. Many experiments[68-72] involving high spins have been performed which support this enhanced probability for photon de-excitation as well as, in some cases, noting a decrease in the amount of energy dissipated by particle emission. There seems, therefore, to be little doubt that particle emission from compound nuclei is supressed by the rotation of the nucleus itself. It is generally agreed that the increased probability for photon emission is a result of an insufficient number of available levels for particle emission. Because a particle will remove about 8 MeV excitation due to its binding energy alone, in addition to its kinetic energy, the compound system is relieved of a large fraction of its excitation with each escaping particle.

Furthermore, the compound nucleus will retain most of its angular momentum following a particle escape, since the kinetic energy of an evaporated particle is quite small compared to the total energy being removed. If the system loses energy only by particle emission and possesses large amounts of angular momentum to begin with, it will soon find itself with relatively low total energy, but retaining a large amount of angular momentum. It will, therefore, be hindered by the lack of available high spin states in any subsequent emissions. Photon emission, on the other hand, presents the possibility of relieving the system of large amounts of angular momentum, even at fairly low energies. Thus a competition is established between the two decay modes. Excitation functions here are a measure of the probability of particle emission and as such, the curves must be shifted toward higher excitation energies by the angular momentum induced competition described above.

An alternate explanation of the effects of rotation on the decay of a compound system has been developed by Kammuri and Nakasima.[29,30] They assume that the angular momentum is removed by particle emission.

This would require increasing kinetic energy of the emitted particles for larger angular momenta. Intuitively, this would effect a shift in the excitation function to higher bombarding (hence excitation) energies. Unfortunately, a quantitative treatment based upon this idea is quite sensitive to several parameters. It is, therefore, uncertain whether such a treatment would be able to explain the experimental result.

Ericson and Strutinski[73] have suggested that the total energy of the compound system is divided into two distinct portions, the true excitation energy of the nucleus and its rotational energy.

$$E^{\ddagger} = E^{*} - E_{rot} \tag{18}$$

where $E^{\ddagger}$ = true nuclear excitation energy

E^{*} = total energy

E_{rot} = energy of rotation

In this treatment the true excitation energy, $E^{\ddagger}$, is the controlling quantity for particle emission, a conclusion supported by Pik-Pichak's[74] calculations for a neutron cascade from a highly rotating nucleus. There, the conclusion was reached that such a cascade would decrease the internal or true excitation energy to a point where particle emission is quite unlikely, while excitational energy in the form of rotation would remain.

The total energy of the compound system, E^{*}, is the same quantity previously described as the excitation energy and defined in Eq. 17.

For a spinning body the rotational energy is given by

$$E_{rot} = \frac{\hbar^2}{2I} \langle J_c(J_c + 1) \rangle \tag{19}$$

where $\hbar^2$ = Planck's constant squared/$(2\pi)^2$

I = moment of inertia

J_c = total angular momentum quantum number of the compound nucleus.

For the present purposes, however, it is more convenient to introduce the rigid sphere moment of inertia, I_{rig}, and an adjustable parameter, k, such that

$$I = k\, I_{rig} \tag{20}$$

We recall that, for a uniform, rigid sphere

$$I_{rig} = \frac{2}{5} mr^2 \tag{21}$$

where m = mass
r = radius = $r_0 A^{1/3}$ for a nuclear sphere
if r_0 = radius parameter = 1.25×10^{-13} cm
A = mass number of the nucleus.

Equation 19 may be rewritten as

$$E_{rot} = \frac{5\hbar^2}{4mr_0^2 A^{2/3}} \frac{\langle J_c(J_c + 1)\rangle}{k} \tag{22}$$

Upon evaluating the constants for a Zn^{64} nuclear "sphere" Eq. 22 becomes:

$$E_{rot} = 3.28 \times 10^{-2} \frac{\langle J_c(J_c + 1)\rangle}{k} \tag{23}$$

Equation 23 will be applied to the experimental data shortly. It is first necessary to obtain a reliable set of curves for the average induced angular momentum in the compound system at various energies.

1. Calculation of Total Angular Momentum

The total angular momentum of the compound nucleus, as a function of energy, $J_c(E)$, is required before it is possible to assess the effects of this motion on the excitation functions. Normally, this quantity is calculated by assuming zero spins for the target and projectile, and then applying classical impact parameter considerations for the target-projectile system. Such a procedure may or may not include realistic

transmission coefficients for each partial ℓ-wave. Often these are taken as unity up to the point where the impact parameter exceeds the maximum interaction distance, whence the T_ℓ's drop rapidly, if not immediately, to zero.

For various reasons that will soon become apparent, the approximations involved in the above procedure are not acceptable in the present discussion, and a more exact method of obtaining the angular momentum must be used. This calculation, like the total reaction cross sections of Sec. IV-A-1, was made with the aid of the OPTIC[58] and ISOMER[64] computer programs. As was mentioned in the previous discussion of the OPTIC calculation, one of the output quantities is a set of transmission coefficients as a function of energy and orbital angular momentum, $T_{(\ell,E)}$. These are a portion of the input for the ISOMER calculation of total reaction cross sections, $\sigma_{(J_c,E)}$, as a function of total angular momentum and energy and including the effects of target and projectile spins. Summing $\sigma_{(J_c,E)}$ over J_c provided the reaction cross sections mentioned in Section IV-A-1. In addition to performing the calculation of partial cross sections, ISOMER also calculates $P_{(J_c)}$, the probability that the compound nucleus has the spin J_c, or

$$P_{J_c} = \frac{\sigma_{(J_c,E)}}{\sum_{J_c=0}^{\infty} \sigma_{(J_c,E)}} \tag{24}$$

Any application of Eq. 23 requires calculation of the quantity $\langle J_c(J_c + 1)\rangle$. Since

$$\langle J_c(J_c + 1)\rangle \equiv \langle J_c\rangle + \langle J_c^2\rangle \tag{25}$$

and since

$$\langle J_c\rangle = \frac{\sum_{J_{c(min)}}^{J_{c(max)}} J_c P_{J_c}}{\sum P_{J_c}} \tag{26}$$

and

$$\langle J_c^2 \rangle = \frac{\sum_{J_c(Min)}^{J_c(max)} J_c^2 P_{J_c}}{\sum P_{J_c}} \qquad (27)$$

it is quite simple to obtain the required quantity (Eq. 25). ISOMER includes $\langle J_c^2 \rangle$ as a part of its output, and manual calculation of $\langle J_c \rangle$ is straightforward. In all cases, the sum over P_{J_c} is unity, while the numerators are summed between

$$J_c(\text{min}) = |I - s|$$

and

$$J_c(\text{max}) = |\ell_{max} + I + s|$$

where I = target spin

s = projectile spin

ℓ = orbital angular momentum quantum number

ℓ_{max} = maximum value of ℓ, as determined by retaining only values of the transmission coefficients greater than 10^{-3}.

and other quantities have been previously described. The results of this calculation are shown in Fig. 18, where $\langle J_c(J_c + 1) \rangle$ is plotted versus E*. Presented in Fig. 19 are the curves shown in Fig. 18 for the p + Cu^{63} and He^3 + Ni^{61} systems where $I = 3/2$ and $s = 1/2$. For comparison, results of a similar calculation, but where target and projectile spins are ignored, are included. Clearly, a rather significant error is introduced by ignoring these spins, especially at the lower energies.

2. Estimation of Rotational Energies

With the acquisition of values for the total angular momentum of the compound system as a function of energy, there remain two undetermined quantities in Eq. 23: the rotational energy and the parameter, k, giving the moment of inertia. Obviously, the most desirable procedure, scientifically, would be to choose the parameter, k, by some means and then proceed

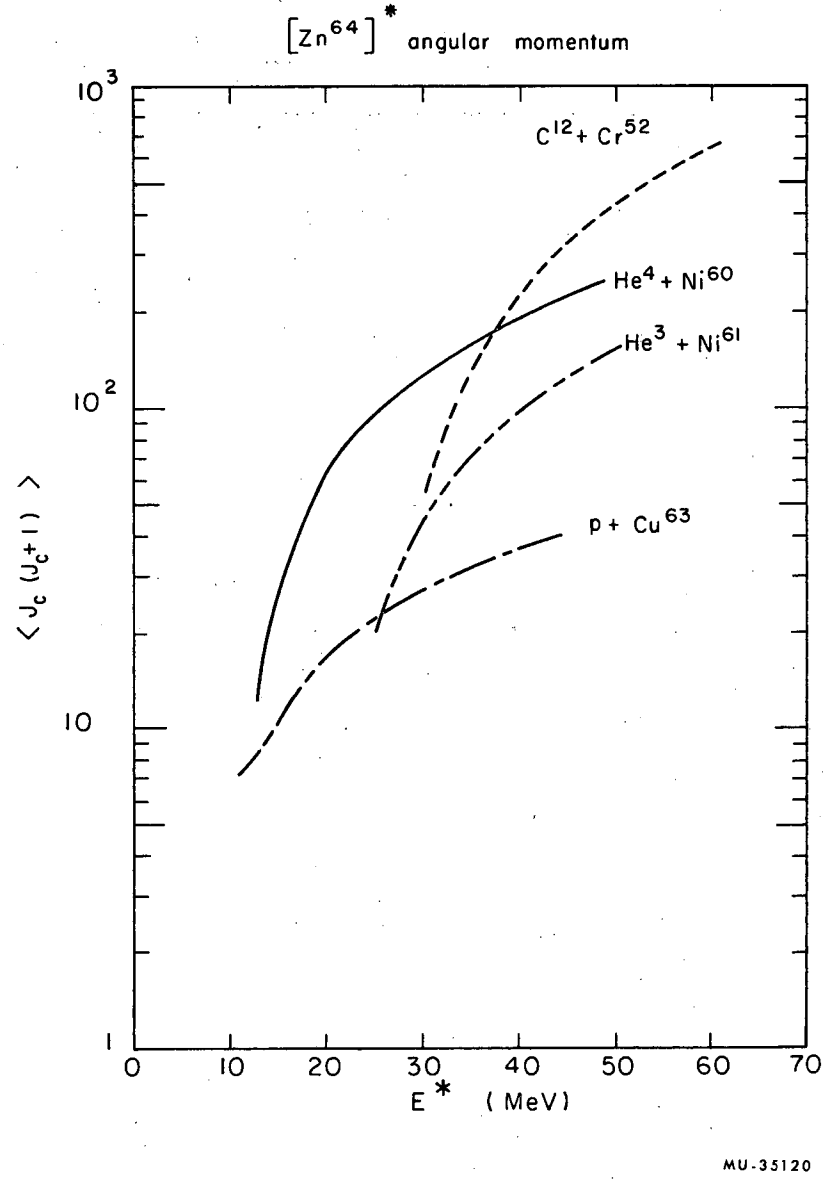

Fig. 18. Average value of the square of the angular momentum of the compound nucleus, $\langle J_c(J_c + 1)\rangle$, as a function of excitation energy for the reactant pairs of interest.

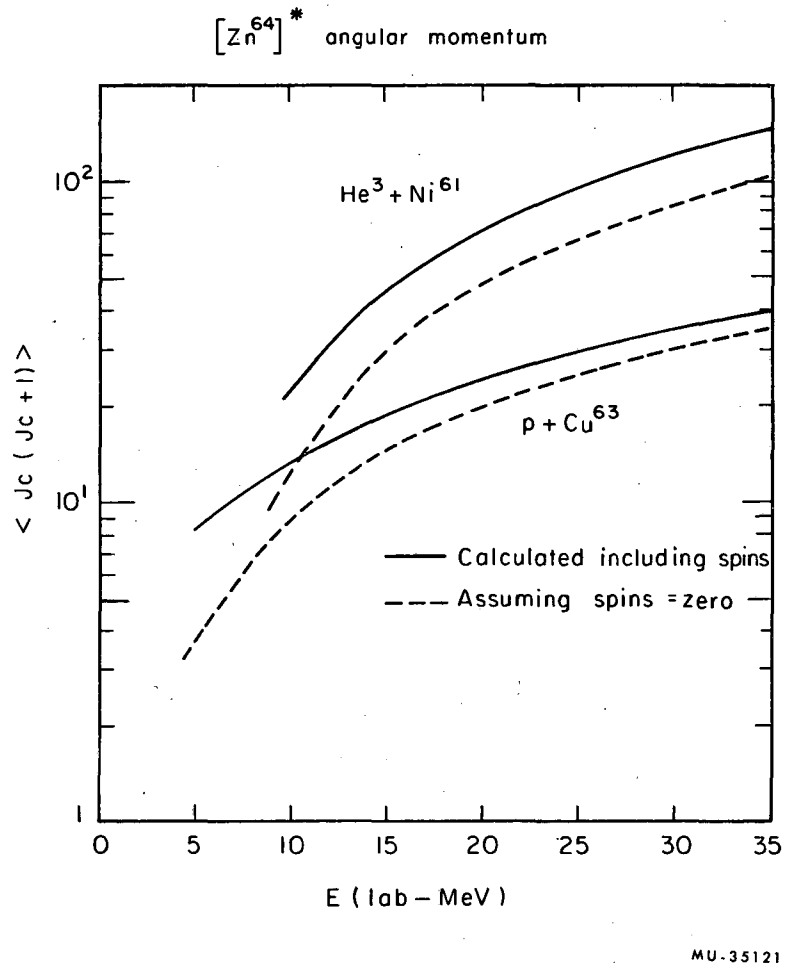

Fig. 19. Average value of the square of the angular momentum of the compound nucleus, $\langle J_c(J_c + 1)\rangle$, as a function of laboratory energy for the $p + Cu^{63}$ and $He^3 + Ni^{61}$ reactions, compared with the corresponding quantity calculated by ignoring target and projectile spins.

to calculate the rotational energy. At high states of nuclear excitation, the theoretical value of the moment of inertia approaches that of a rigid sphere. At lower states of excitation, collective motion of the nucleons comprising the compound system is retarded by the pairing forces. Thus the value of the moment of inertia is lowered below that of a rigid sphere. One would expect that at the levels of excitation being investigated here that k would very nearly equal one, i.e. $I = I_{rig.}$ Unfortunately such has been experimentally shown not to be the case.[75,76] As a result any selection of a value for k must be uncertain, making the scientifically desirable process unfeasible. Therefore, the reverse procedure will be adopted—that is, an experimental estimate of the rotational energy will be made and the corresponding value of the moment of inertia parameter calculated. These experimental k's can then be compared in the hope of discovering a correlation between them.

The experimental excitation functions for any particle-induced nuclear reaction have, presumably, been shifted to higher energies by the unavoidable angular momentum effects. The size of this shift should be the rotational energy of the system. Therefore, to find the rotational energy experimentally it is necessary to know the position of the excitation function in the absence of any rotational energy. Failing this, the non-rotating compound nucleus may be approximated by one possessing negligible angular momentum. Such a compound nucleus could be produced by photo-excitation.

Sagane[66] has determined relative excitation functions for photo-excitation of Zn^{64}, and these curves will provide the zero spin system which will be used as a reference in the calculation of the moments of inertia. These curves were shown, along with the present experimental results, in Figs. 15, 16, and 17. Taking the peaks of these curves as being the most characteristic point, and as best representing the compound nuclear portion of the reaction mechanisms, an expression relating the energy of the photon curve to the various particle curves can be obtained. In the Target(X,pn)Cu^{62} system for example,

$$E_{h\nu} \approx E^*_p - 2.5 \text{ MeV} \approx E^*_\alpha - 3.8 \text{ MeV} \approx$$

$$E^*_{He^3} - 8.5 \text{ MeV} \approx E^*_{C12} - 15.5 \text{ MeV} \qquad (28)$$

where E^*_x = excitation energy calculated from Eq. 17, and where the differences are taken from the various peaks. This discrepancy between experimental peak positions and the position characteristic of a virtually zero angular momentum compound nucleus represents the rotational energy of the system as defined in Eq. 18. From these rotational energies, the calculated angular momenta, and Eq. 23, values of k may be obtained. These quantities are summarized in Table VII.

Within the rather large limits of error inherent in the determination of peak energies and the unknown energy scale reliability of Sagane's results, an inexact determination of k is expected. Shifts, or rotational energies, determined from the (x,n) curves are too much in error to be useful. At higher energies, the uncertainties account for 10 to 20% of the energy shift, and some definite trends in the calculated k values are noted. Both the proton- and He^3-induced reactions show values of k near 0.3, while the alpha particle reactions have k's which are essentially unity. Carbon ion reaction results are intermediate between the two. Within the error limits of this data, it is not possible to state positively whether alpha and carbon reactions differ, or whether both produce values of k somewhere around 0.8 ± 0.2. In any case, there is an unmistakable difference between these reactions and the proton- and He^3-induced reactions.

If the supposition that the peaks in the excitation functions correspond to a uniform state of excitation of the compound system is correct, and if differences between these are, in fact, due to energy in the form of rotation, then it is not immediately clear why this division of results should occur. If k is, as the collective model informs us, related to the pairing forces in the nucleus, and if the presence of these pairing forces depends on the overall degreee of nuclear excitation, then a uniform value for the

Table VII. Results of reduced moment of inertia calculations.

Reaction	E* peak	$E_{rot(expt)}$	$\langle J_c(J_c + 1)\rangle$	$k = I/I_{rig}$
$Cu^{63}(p,n)Zn^{63}$	18.5 ± 1	0.8 ± 1.4	15.3	0.63 ± 1.10
$Cu^{63}(p,2n)Zn^{62}$	32.0 ± 1	4.5 ± 1.4	29.8	0.22 ± 0.68
$Cu^{63}(p,pn)Cu^{62}$	30.0 ± 1	2.5 ± 1.4	28	0.37 ± 0.21
$Ni^{60}(\alpha,n)Zn^{63}$	19.6 ± 1	1.9 ± 1.4	56	0.96 ± 0.71
$Ni^{60}(\alpha,2n)Zn^{62}$	32.5 ± 1	5.0 ± 1.4	149	0.98 ± 0.27
$Ni^{60}(\alpha,pn)Cu^{62}$	31.3 ± 1	3.8 ± 1.4	133	1.15 ± 0.42
$Ni^{61}(He^3,n)Zn^{63}$	---	---		
$Ni^{61}(He^3,2n)Zn^{62}$	37.0 ± 1	9.5 ± 1.4	82	0.28 ± 0.041
$Ni^{61}(He^3,pn)Cu^{62}$	36.0 ± 1	8.5 ± 1.4	77	0.30 ± 0.049
$Cr^{52}(C^{12},n)Zn^{63}$	---	---		
$Cr^{52}(C^{12},2n)Zn^{62}$	43.0 ± 2.5	15.5 ± 2.7	292	0.62 ± 0.11
$Cr^{52}(C^{12},pn)Cu^{62}$	43.0 ± 2.5	15.5 ± 2.7	292	0.62 ± 0.11
$Zn^{64}(h\nu,n)\ Zn^{63}$	17.7 ± 1			
$Zn^{64}(h\nu,2n)Zn^{62}$	27.5 ± 1			
$Zn^{64}(h\nu,pn)Cu^{62}$	27.5 ± 1			

moment of inertia would be expected. Instead, the results show at least two distinctive values. If, perchance, k is not characteristic of the nucleus as a whole, but is somehow connected to the total angular momentum, the observed grouping of values may be explained, but the order of k values would not be predicted. This is, therefore, an unlikely explanation. The most obvious explanation is the zero reactant spins in the cases of He^4 and C^{12}, as opposed to the non-zero spins in the other instances.

At this point it is important to recall that the constant, k, is essentially only an artifact. Under the assumptions discussed above, one cannot intelligently talk of differences in the moment of inertia of similar compound nuclei. We are, in reality, merely using the calculation of k as a convenient means of expressing what appears to be a real discrepancy between the actual angular momentum and the calculated angular momentum in this system. Furthermore, <u>any</u> treatment of angular momentum effects which attempts to explain the observed peak positions as a function of J_c will be hard-pressed to explain the near superposition of the proton and alpha-particle curves, and the position of the He^3 curves relative to the other three. Theory remains inconsistent with experiment if one considers the possibility that the He^4 and C^{12} curves are displaced toward lower energies, while the He^3 and proton curves are reasonably "normal." Such an argument is suggested by the values of 0.3 for the constant, k, obtained in the latter cases, but is refuted by the lack of a mechanism suitable to cause such a "negative" energy shift.

Calculation of the angular momentum quantum numbers for the compound nucleus has been done according to the best modern understanding of the interaction processes. Such understanding may not be sufficient in the present case, especially where projectile and target spins must be coupled to the orbital angular momentum. The effect of ignoring these spins is to create an even greater problem in the interpretation of these results. The system is behaving as if the true spin is greater than that calculated, and by ignoring these spins, theory and experiment diverge even more. While the peak positions, themselves, are certainly in doubt, it is difficult to accept the error required to bring these values of the

parameter, k, into agreement. This is especially so with the proton and alpha reactions, where range-energy curves, beam energies, and foil thicknesses are quite well known. It seems, therefore, that neither experimental nor theoretical difficulties can account for the observed parameter variation.

Arbitrary superposition of the peaks, as was done by Ghoshal, does demonstrate their similarity, and is normally considered as a verification of the independence postulate. It is quite possible that, ignoring angular momentum effects, the alpha and proton curves are close enough together so that no arbitrary shift is required, and that these two curves represent a special case in which the prediction of the simple theory is demonstrated. The addition of the He^3 and C^{12} curves to the picture, however, presents a further complication. In these cases not even the inclusion of angular momentum considerations will allow a comparison of the type represented by Eq. 10, without the introduction of an arbitrary energy shift. Clearly something is awry, and it may very well be the application of the independence postulate to this set of reactions as a whole. In the next section, it will be seen that the shapes of these curves are not only similar, but also very much like curves predicted according to evaporation theory. In previous sections it has been seen that recoil-range experiments and knowledge of similar interactions in the medium mass region are consistent with the compound nuclear reaction theory. We are, therefore, probably dealing with a system that is predominantly compound nuclear in nature, but does not, in toto, decay independently from its mode of formation.

A further series of experiments designed to establish the degree in which these reactions differ from other predictions of statistical theory would be of value in an attempt to resolve this conflict quantitatively. For the present, however, it will suffice to be aware that the system being investigated seems to be sensitive to the way it was formed, and that its mode of decay seems to depend on the origins of its rotational energy. If it is formed from a system carrying only orbital angular momentum, the relative energy shift due to its rotation is not as great as

if the system were spinning before the interaction occurred. While present understanding does not permit quantitative explanation of this difference, the concept is quite useful in attempting to understand results of other "iso-compound-nuclear" experiments. This topic will be discussed more fully in Sec. V of this work.

C. Shape of the Excitation Functions

Throughout much of the preceding discussion references have been made to the shape of an experimental curve. Often the adjective compound-nuclear accompanied these references. In this section a brief review of an approximate method of obtaining statistical evaporation probabilities will be presented and the results compared to the experimental curves. Where better calculations are available, they will also be presented.

The $[Zn^{64}]^*$ system has been subjected to a Monte Carlo evaporation calculation by Dostrovsky, Fraenkel, and Friedlander[77] in the cases of proton and alpha induced reactions. This is presumably the best available theoretical estimation of the shapes of these curves. They are presented in Figs. 20 and 21 along with the corresponding experimental results. The agreement shown in these comparisons is considered satisfactory and provides the basis for referring to these results as essentially compound nuclear in nature. The discrepancy on the energy scale is most probably due to uncertainty in the calculational procedure, since it is in the "wrong" direction. For the experimental curves to appear at lower energies than actually predicted by the statistical model, the compound nucleus must be emitting particles while, at the same time, having insufficient energy to do so. Conversely, if non-statistical processes are invoked to account for the "early" appearance of the experimental curves, one is hard pressed to find such a process with sufficient probability to match the observations. With no logical alternative, it may be assumed that the peak in an excitation function must occur at or after the statistical model position. If it does not, the fault must lie in the uncertainties inherent in the calculations.

In cases of He^3 and carbon ion reactions, no such calculation has been performed. In order to obtain an approximate theoretical curve a

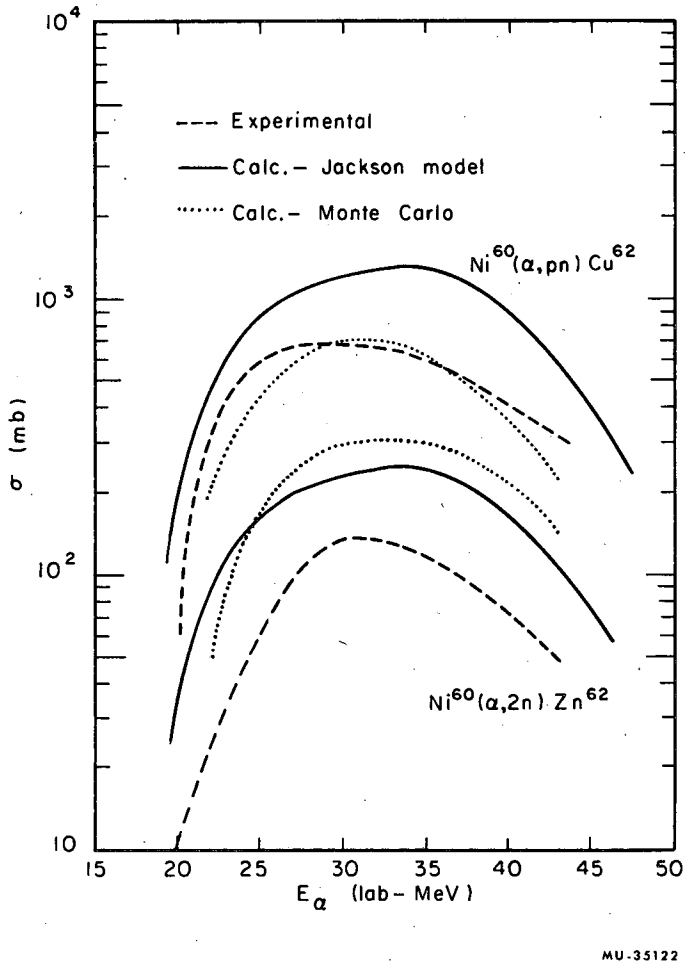

Fig. 20. Calculated excitation functions for the $Ni^{60}(\alpha,2n)Zn^{62}$ and $Ni^{60}(\alpha,pn)Cu^{62}$ reactions compared to the experimental curves. Monte Carlo calculations are from ref. 77.

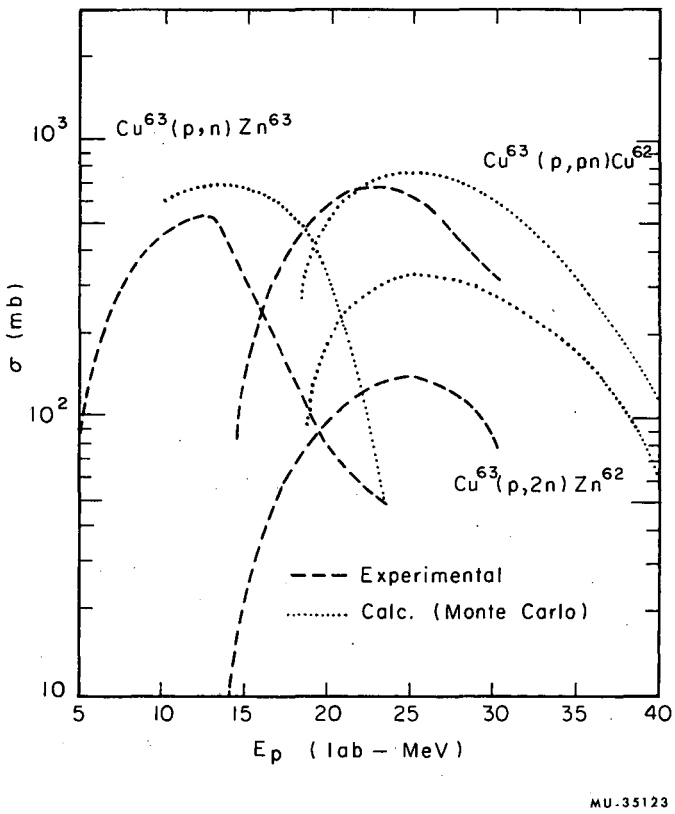

Fig. 21. Calculated excitation functions for the $Cu^{63}(p,2n)Zn^{62}$ and $Cu^{63}(p,pn)Cu^{62}$ reactions compared to the experimental curves. Monte Carlo calculations are from ref. 77.

modified Jackson model calculation has been performed.[78,79] In this model the cross section is written as

$$\sigma_{(B,xn)} = \sigma_R(E_B)\, G_1\, G_2 \ldots G_x\, P_{xn}(E^*) \qquad (29)$$

where $\sigma_{(B,xn)}$ = cross section for the reaction, $\text{Target}(B,xn)_{30}{}^{ZN}{}^{64-x}$

$\sigma_R(E_B)$ = total reaction cross section

G_X = branching ratio for emission of the xth neutron

$P_{xn}(E^*)$ = probability of evaporating exactly x neutrons.

In the approximation being considered here, the limitation of the Jackson model to neutrons is not serious. This is demonstrated by the similarity in shape of the experimental results for the (B,pn) and (B,2n) reactions. Therefore, the Jackson model may be used to calculate the probability for emission of "x" particles, protons or neutrons. This probability may then be divided according to the ratio of the peaks of the experimental curves for comparison purposes.

The probability that exactly x particles are emitted is

$$P_{xn}(E^*) = I(\Delta_x, 2x-3) - I(\Delta_{x+1}, 2x-1) \qquad (30)$$

where $I(z,n)$ is Pearson's incomplete gamma function[80] and

$$\Delta_x = \left(E^* - \sum_x \frac{B_i}{T}\right)$$

if B_i = binding energy of the ith particle

E^* = excitation energy

T = nuclear temperature.

The expression for Δ_{x+1} is similar in form to that for Δ_x. In this system, the effects of gamma de-excitation should become noticeable only after emission of the second or third particle, because of the high excitation of the compound nucleus. Therefore, particle emission is the

only decay mode that need be considered, and the branching ratios (G_x) may be taken as unity. Furthermore, the basic assumption that the nuclear temperature remains constant throughout the evaporation process will be adopted. This quantity does not significantly affect the shape, but serves to alter the magnitude of the calculated cross sections.

The Jackson model presumably estimates the sum of all two-particle emission probabilities. If experimental results were available for the (B,2p) reaction, then by adjusting the nuclear temperature it should be possible to obtain a reasonable fit to the sum of the experimental two particle emission reaction cross sections. Unfortunately, no such results are available for this system (or for the $[Cu^{63}]^*$ one particle emission cross sections). This is, of course, due to the fact that the product formed by $Zn^{64} \longrightarrow 2p$ or $Cu^{63} \longrightarrow p$ emission, is Ni^{62}, a stable nuclide. It might be possible to estimate $\sigma_{(Cu^{63} \longrightarrow p)}$ by assuming $\sigma_R = \sigma_{(Cu^{63} \longrightarrow p)} + \sigma_{(Cu^{63} \longrightarrow n)}$ but no measurement of the cross section for neutron emission from a $[Cu^{63}]^*$ compound nucleus has been reported insofar as this writer is aware. Similar arguments prevent the estimation of $\sigma_{(Zn^{64} \longrightarrow 2p)}$ from available data for the $[Zn^{64}]^*$ compound nucleus. Since no allowance can be made for (B,2p) reactions, the calculated cross section magnitude is not significant—only the shape, and therefore the nuclear temperature, T = 2.5 MeV, was adopted and used throughout.

To test the accuracy of this procedure for estimating shapes, the excitation functions for the (α,2n) and (α,pn) reactions were calculated. These results are compared to the Monte Carlo calculations and the experimental results in Fig. 20. There it is seen that the procedure is reasonably good. The curves follow the outline of the (α,2n) reaction well and that of the (α,pn) reaction somewhat less well, especially at higher energies. The experimental curves are somewhat more narrow than the evaporation calculation predicts. These differences might be corrected if the division of the calculated evaporation curve into its several components could be improved. Comparison with the Monte Carlo calculation shows fairly good overall agreement in shape and an energy difference of 1.5 to 2 MeV—well within the uncertainties of these calculations. The agreement as to peak position is only fair, the theoretical

curve peaking at 2 to 3 MeV higher energies than the experimental curve. As is the case for the Monte Carlo calculation, this discrepancy most probably represents the uncertainty in the calculational procedure. Clearly, the modified Jackson model is capable of providing a reasonably good approximation to the shapes of both the experimental and the Monte Carlo curves.

The experimental and calculated curves for the $He^3 + Ni^{61}$ and $C^{12} + Cr^{52}$ are compared in Figs. 22 and 23. Immediately apparent is the similarity in curve shape, even though the calculated curves are too broad. The calculated curves for the carbon ion induced reactions have been shifted by 5 MeV so that their shapes may be more easily compared to the experimental curves. In the case of the He^3 curves, no energy shift has been made. The effects of competition reactions are obvious in Fig. 23, where the carbon ion reactions do not fall back rapidly enough following the peak. In all other curves the calculated values form a kind of envelope around the experimental curves.

Perhaps a comment on the relative breadth of the corresponding excitation functions is in order. Because of the nature of the calculational procedure, all reactions are grouped according to number of emitted particles. Such a grouping appears only by accident in nature, where the probability for a given reaction rises from threshold, peaks, and falls off according to the dictates of the energetics of the system within its allotted portion of the total reaction cross section. Normally the energetics introduces a degree of variation in the curve position along the energy axis. Therefore, an experimental curve may not be able to rise as rapidly from threshold as might be expected from evaporation considerations due to other reactions competing for their share of the total cross section. Similarly, an experimental curve may fall away more quickly than this simple model would indicate. It would be quite surprising if this simple theory were not broader than the experimental results for compound statistical reactions.

In view of the relative uncertainties of the calculation, it is hardly worth-while to dwell on relative peak positions. The carbon-ion calculation (Fig. 23) may, indeed, indicate a real shift in the energy

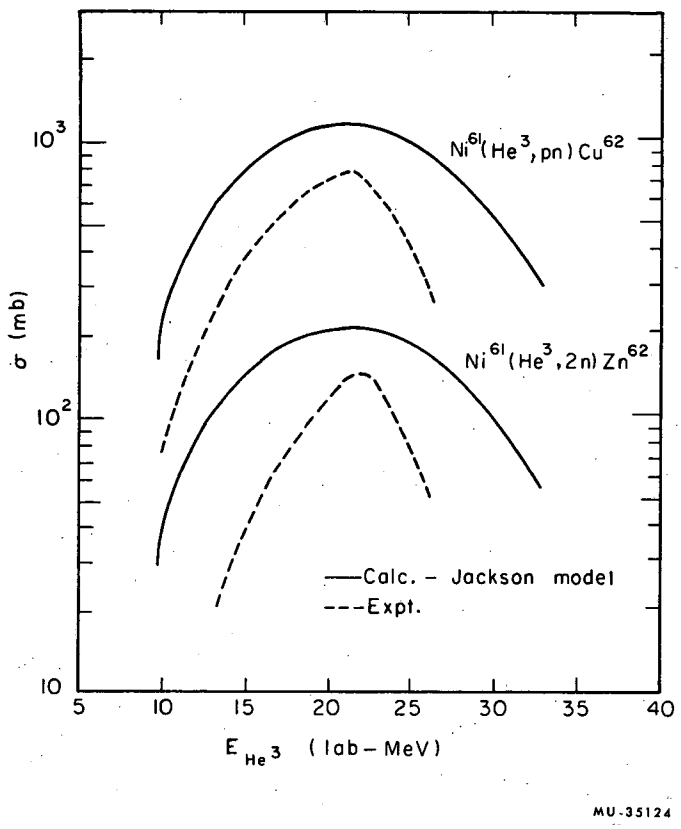

Fig. 22. Calculated excitation functions for the $Ni^{61}(He^3,2n)Zn^{62}$ and $Ni^{61}(He^3,pn)Cu^{62}$ reactions compared to the experimental curves.

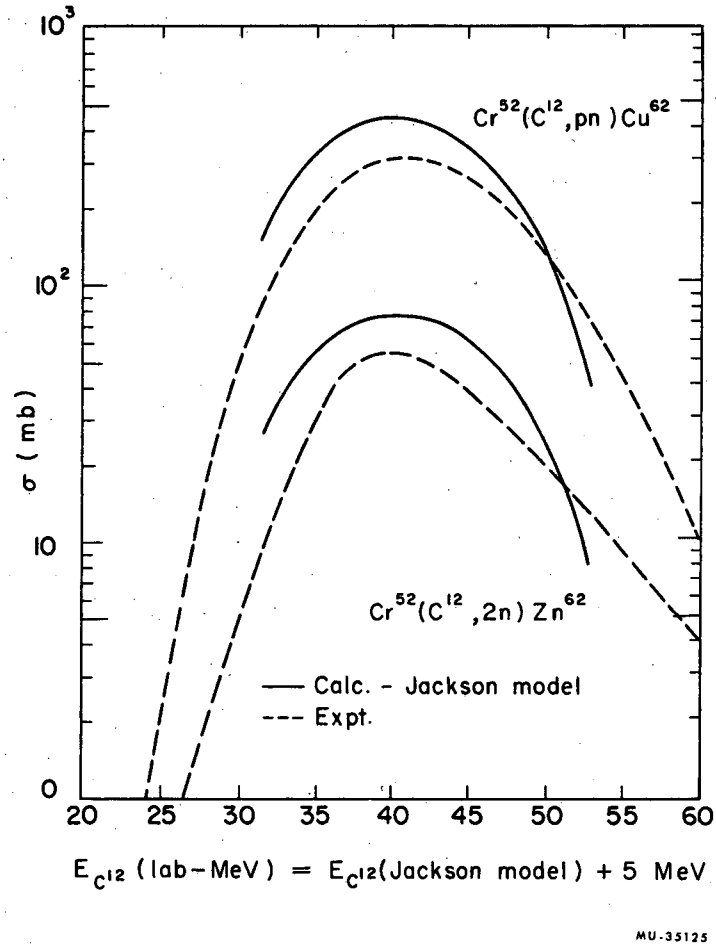

Fig. 23. Calculated excitation functions for the $Cr^{52}(C^{12},2n)Zn^{62}$ and $Cr^{52}(C^{12},pn)Cu^{62}$ reactions compared to the experimental curves.

scale. Other comparisons are indeterminate. Certainly no statement based on these results concerning angular momentum effects is possible, perhaps with the exception that the carbon reactions are shifted in the right direction. These calculations do, however, serve to support the contention that the reactions being investigated are primarily of a compound nuclear nature.

V. "ISO-COMPOUND-NUCLEAR" EXPERIMENTS

Basic to the theory of compound nuclear reaction is the so-called "independence postulate". Ghoshal[10] was the first to test this portion of the reaction theory by forming a compound system in two ways. The similarity of the corresponding excitation functions was accepted as a demonstration of the independence postulate. Since Ghoshal, several experimenters have performed "iso-compound-nuclear" studies using different compound systems.[11-28] It seems appropriate here to review these results in light of the present re-examination of Ghoshal's experiment, and to attempt to compile this body of experiments in such a way as to demonstrate their similarities (and differences).

This task is not a straightforward one, since besides the compound nuclear interaction there are various other kinds of interactions taking place. The observed excitation functions are the sum of contributions from CN, direct interaction (nuclear transfer) and partial CN mechanisms. The (α,n) and (p,n) curves of Ghoshal show a high energy tail which is probably due to a direct process which retains appreciable cross section long after the statistical competition in the CN would all but prohibit these reactions. Similar results have been seen by many experimenters. See, for example, the $Fe^{54}(\alpha,p)Co^{57}$ and $Fe^{54}(\alpha,n)Ni^{57}$ work of Houck and Miller[46] and the $Cu^{63}(p,pn)Cu^{62}$ studies of Meadows.[11]

On the other hand, heavy ion reactions involving products with a mass near that of the CN do not show these tails (see for example Read, Ladenbauer-Bellis, and Wolfgang[50] or Karamyan, Gerlit, and Myasoedov)[52] because of their statistical nature. Alpha-particle inelastic scattering experiments have shown forward peaking in the differential cross sections.[81,82] However, these scattering experiments also demonstrated that CN mechanisms predominate in the backward hemisphere. Forward peaking is also observed, for example, in $Cu^{63}(\alpha,p)Zn^{66}$ reactions of Eisberg, Igo, and Wegner.[83] Direct comparisons of the two kinds of measurements cannot be made since, in general, one cannot perform radiochemical reaction studies on the same systems used for inelastic scattering. It is therefore only possible to conclude that both non-CN and CN interactions are

important in this region, and that either kind of experiment serves to investigate only a portion of the total picture. Furthermore, non-compound processes do not appear to affect the similarity in shape of "iso-compound-nucleus" excitation functions in any of the systems so far studied by a Ghoshal-type experiment.

The results of the work of Stearns[25] with reactions of the type $A(x,y)B$, where $x = p, \alpha, C^{12}$ and $y = \alpha n, \alpha 2n, 2p, 2n$, which lead to the $[Cu^{63}]^*$ compound nucleus show clearly that some direct processes do contribute to the excitation functions. In particular, she showed that there seems to be a preference for re-emission of the incident particle from the CN, thus enhancing the $Ni^{62}(p,2p)Co^{61}$ cross section as compared to the $Co^{59}(\alpha,2p)Co^{61}$ cross section. Similar results were obtained for the Co^{58} and Co^{57} yields, showing enhancement of the $(x,\alpha n)$ or $(x,\alpha 2n)$ for the case of $x = \alpha$ over that for $x = p$. Both of the latter cross sections were actually higher than the statistically calculated value.

Comparisons of excitation functions involving "iso-compound-nuclear" reactions do not suffer greatly from the ad-mixture of reaction mechanisms determining their shape. These comparisons are designed to investigate only the compound nuclear portion of the excitation function and therefore are made in the vicinity of the peak in the cross sections for each reaction being considered. Non-similarity in shape, due to non-compound processes, is generally apparent only in the high energy tails and is normally ignored in analysis of these experiments. Since most of the comparisons have been made using proton-, alpha particle- or heavy ion-induced reactions the non-compound contribution would not be expected to be very great and the similarity in shape of the experimental excitation functions, over a wide target mass range, indicates that this expectation is essentially correct. It is somewhat disturbing to note that even when comparisons are made between reactions expected to be predominatly non-compound-nuclear and reactions expected to be predominantly compound nuclear, the similarity in shape is still present to some extent.[25] No clear explanation presents itself for this implied similarity in shape of excitation functions corresponding principally to different reaction

mechanisms. Obviously, the shape of a curve is not, in itself, proof of compound nuclear mechanisms. Additional information from scattering or recoil range experiments is required to fix the true reaction mechanism.

Another problem, discussed in Sec. IV, is that of the energy discrepancy between calculated and experimental excitation energies. In the oldest iso-compound-nuclear experiments this problem was ignored due to relatively inaccurate mass tables.[10] With the determination of better mass values, the problem began to receive attention,[17-24] and the most recent such experiments invoked angular momentum effects to explain the observed discrepancies.[25-27] Of these, only two treatments of the effect present themselves. Stearns[25] adopted a procedure similar to that presented previously in Sec. IV-B in which a division of energy between excitation and rotation is assumed. Unfortunately, this calculation was made without a zero spin compound nucleus reference point, and the moment of inertia that is obtained is representative only of the difference between the curves and not of the actual physical shift. Thus it is quite different from the $[Zn^{64}]^*$ case discussed previously. Furthermore, the calculations of angular momenta are not made with the same assumptions in these two cases. About all that can be said is that the value of parameter, $k = 0.5$, is in rough agreement with the lower of the two parameters obtained from the $[Zn^{64}]^*$ calculations. If a zero spin reference were available for $[Cu^{63}]^*$ the agreement would be expected to improve.

Grover and Nagle[27] have studied the (x,n) and (x,2n) products from the $[Po^{210}]^*$ compound nucleus. Their results are reported as ratios, $R_x = \frac{\sigma_{(x,2n)}}{\sigma_{(x,n)} + \sigma_{(x,2n)}}$ for $x = \alpha$ or p. It is clearly shown that at all values of excitation energy, $R_\alpha > R_p$. This discrepancy, while appearing to be in the wrong direction when compared to the $[Cu^{63}]^*$ or $[Zn^{64}]^*$ experiments, is explained by taking into account the different angular momentum distributions of $[Po^{210}]^*$ produced by the two bombarding particles. They find that their results agree quite well with the compound nucleus model if they allow for increased gamma ray de-excitation at the expense of particle emission as angular momentum is increased, thus shifting the excitation function to higher energies. Such a treatment,

if applied to the $[Zn^{64}]^*$ system, would not provide a solution to the problem, since here the order of peak shifting does not follow the calculated angular momentum.

It is interesting to note that the two sets of experiments leading to $[Po^{210}]^*$ combine to provide a qualitative picture of angular momentum effects. At low energies Grover and Nagle find essentially that the proton curve is shifted to higher excitation energies than the corresponding α peak. This is presumably due to the fact that at lower energies more angular momentum is imparted to the compound system in the p + Bi^{209} than in α + Pb^{206} due to the I = 9/2 spin of Bi^{209}. Furthermore, the results for Zn^{64} indicate a relatively greater shift is expected from the spin effects than from orbital angular momentum effects. As energy is increased, the α + Pb^{206} begins to impart more and more angular momentum to the compound system. The (α,xn) curves are shifted to higher energies and soon appear at excitation energies greater than those of the corresponding proton-induced reaction. This is the situation found when Kelly's $Bi^{209}(p,xn)$ excitation functions[84] are compared with John's curves[17] for the $Pb^{206}(\alpha,xn)$ reactions.

Somewhat the same problem is found when the Fe^{56} + α curves of Tanaka et al.[24] are compared with those of Sharp, Diamond and Wilkinson[23] for Co^{59} + p. In this system leading to a $[Ni^{60}]^*$ compound nucleus, it is found that the proton curves must be shifted less than would be expected from mass values. The explanation for this reversal from other such comparisons in this mass region[11-16,22,25,26] may be similar to that for the $[Po^{210}]^*$ case discussed above. The Co^{59} nucleus has a spin, I, of 7/2 while the Fe^{56} has zero spin. If the effects of this high target spin combined with the orbital angular momentum brought in by the proton are great enough to overcome the large angular momentum induced by the alpha particle, then the proton curves should appear at an energy higher than that for the alpha curves, explaining this experimental observation. Judging by the alpha curves' appearance below the Helium-3 curves in the present work, this may indeed be the case. At elevated energies, the difference should be less and should eventually revert to the more normal

appearance of the $[Zn^{64}]^*$ or Stearns' curves. Again the proximity of the positions of the proton and alpha curves in the current study, especially at low energies, supports this contention. These effects are simply magnified by the higher spins in the $[Ni^{60}]^*$ system.

The experimental results of Porile et al.[26] for the Ge^{70} compound nucleus show the curves representing the $\alpha + Zn^{66}$ reaction are some 3 MeV above the corresponding curves for the $p + Ga^{69}$ reaction. This pair of reactions is very nearly identical to the $\alpha + Ni^{60}$ and $p + Cu^{63}$ reactions leading to $[Zn^{64}]^*$, in aspects such as target and projectile spins, energy range and masses. Thus it is encouraging to find the energy shift in the Ge^{70} system to be essentially the same as that in the Zn^{64} system.

In the comparison by Chen and Miller[22] of the $\alpha + Sc^{45}$ and $d + Ti^{47}$ reactions leading to a V^{49} compound nucleus, the average target and projectile spin is higher for the alpha reaction, but both the deuteron and the Ti^{47} target have appreciable spins, averaging fairly near that of the Sc^{45} target. This system, therefore, allows some estimate of the effect of concentrating spin on the target, as opposed to splitting it between target and projectile. In these results, the deuteron peak appears at higher energies than the alpha peak for low energy reactions, while the reverse is true at higher energies. Thus, evidence is provided that splitting the spins between the reactants will produce a greater effect on the energy scale of the excitation functions than concentrating this spin. In other words, the angular momentum effects appear to be greatest if both particle and target possess spins, less if only one partner has a spin, and least if both reactants are spinless.

Several high energy proton induced reactions have been compared to heavy ion-induced reactions in the low mass region.[18-21] Due to the low energy of the heavy ions, the low mass of the targets, and the high proton energies required, these experiments are not of the same type as those discussed above. The energetics for the heavy ion reaction, combined with the fact that target and projectile have equivalent masses, preclude very high angular momenta in the resulting compound nucleus. On the other hand, the proton reactions being studied require rather high energies, and many

of the proton excitation functions in these comparisons are predominantly non-compound-nuclear in nature. Therefore, no real comparison of the type presented for medium weight compound nuclei will be made.

All of the iso-compound-nuclear comparisons that have been made are listed in Table VIII. An attempt is made to present enough of the significant features of these experiments so that it is possible to qualitatively apply the spin corrections deduced from the present work. It is seen that in every case the predicted order of the peaks with increasing energy is the same as that observed experimentally. Thus, although current understanding is not sufficient to provide a theoretical basis for quantitative understanding of the angular momentum effects, the considerations presented in this paper do allow a qualitative understanding.

Table VIII. Summary of iso-compound-nuclear reactions.

Compound nucleus	Reactions	I_b	I_T	Products	E* range	Exp't'l order (E*)	Spin predicted order (E*)	Refs.
$_{12}Mg^{24}$	$p + Na^{23}$	1/2	3/2	pn	~ 20	~ even	$p\text{-}C^{12}$ or	18
	$C^{12} + C^{12}$	0	0				~ even	19
$_{13}Al^{26}$	$p + Mg^{25}$	1/2	5/2	2p	30-35	p, C^{12}	$p\text{-}C^{12}$	18
	$C^{12} + N^{14}$	0	1	2n2p				19
$_{13}Al^{26}$	$p + Mg^{25}$	1/2	5/2	2p	20-25	p, C^{12}	$p\text{-}C^{12}$, or	20
	$C^{12} + N^{14}$	0	1	$\alpha;2\alpha$			~ even	
$_{14}Si^{28}$	$p + Al^{27}$	1/2	5/2	3pn	~ 70	uncertain	$p\text{-}C^{12}$	21
	$C^{12} + O^{16}$	0	0					19
$_{23}V^{49}$	$\alpha + Sc^{45}$	0	7/2	n;2n	~ 23	α,d	α,d	22
	$p + Ti^{47}$	1	5/2	2p;αn	~35	d,α	d,α	
$_{28}Ni^{60}$	$p + Co^{59}$	1/2	7/2	pn;3n	25-45	α,p	α,p	23
	$\alpha + Fe^{56}$	0	0	p2n;αpn				24
$_{29}Cu^{63}$	$p + Ni^{62}$	1/2	0	αn	36-48	p,α	p,α	25
	$\alpha + Co^{59}$	0	7/2	α2n				
	$C^{12} + V^{51}$	0	7/2	2n				

(continued)

Table VIII. Summary of iso-compound-nuclear reactions. (Continued)

Compound nucleus	Reactions	I_b	I_T	Products	E* range	Exp't'l order (E*)	Spin predicted order (E*)	Refs.
$_{30}Zn^{64}$	p + Cu^{63}	1/2	3/2	n	15-50	p,α,He^3,C^{12}	(p,α,He^3,C^{12})	10-16 and present experiment
	α + Ni^{60}	0	0	2n		~even		
	He^3 + Ni^{61}	1/2	3/2	pn				
	C^{12} + Cr^{52}	0	0					
$_{30}Zn^{66}$	α + Ni^{62}	0	0	pn	~ 35	~ even	~ even	11
	p + Cu^{65}	1/2	3/2					12
$_{32}Ge^{70}$	p + Ga^{69}	1/2	3/2	n;p2n	20-40	p,α	even to p,α	26
	α + Zn^{66}	0	0	αpn;3n				
				pn;αn				
Po^{210}	p + Bi^{209}	1/2	9/2	2n;3n;4n	to~45	p,α ~even	p,α	17
	α + Pb^{206}	0	0					
Po^{210}	p + Bi^{209}	1/2	9/2	$\frac{\sigma_{2n}}{\sigma_{2n} + \sigma_n}$	below 17.5	α,p	α,p	27
	α + Pb^{206}	0	0					
Po^{211}	α + Pb^{207}	0	1/2	fission	~ 35	~ even	uncertain	28
	p + Bi^{209}	1	7/2					

VI. CONCLUSIONS

The major conclusions reached in this work are:

1. The reactions of p, α, He^3, and C^{12} with the appropriate targets to produce a $[Zn^{64}]^*$ compound nucleus proceed predominantly through a compound nuclear reaction mechanism. Only a small portion of the cross sections are attributable to non-compound processes.

2. The ratios $\sigma_{(x,w)}/\sigma_R$ are effectively constant for a given exit channel, w, and superposition of the curves is possible if the energy scale is shifted arbitrarily. The shape of the experimental curves for a given product is reasonably uniform.

3. The excitation functions are not shifted upward in energy in proportion to $\langle J_c(J_c + 1)\rangle$. Both the $He^3 + Ni^{61}$ peaks and the $p + Cu^{63}$ peaks are shifted to a greater degree than predicted on this basis. This discrepancy is attributed to the enhanced effect of spin angular momenta as compared to orbital angular momenta.

4. Results such as presented in conclusion 2 above, are usually taken as evidence which verifies the independence postulate. However, the necessity of an arbitrary energy shift, and the indication, (conclusion 3) that the decay of the compound system is influenced by its mode of formation tends to discount the applicability of the concept of independence to this system as a whole.

5. The importance of various sources of the total angular momenta in the compound nucleus may be ordered according to increasing energy shift produced in an excitation function. The observed order is

   a) the orbital angular momentum of the projectile-target system, then,

   b) the spin angular momentum of one of the two reactants, then,

   c) the interaction of spin angular momenta of both target and projectile.

6. Application of conclusions 3 and 5 to the literature produces general agreement in the results of iso-compound-nuclear experiments. The uncertainty in magnitude and direction of these results is therefore removed.

ACKNOWLEDGMENTS

It is a pleasure to acknowledge the continuing interest and helpful advice of my research director, Dr. Samuel S. Markowitz.

Several discussions with Dr. John Mahony, Dr. Paul Croft, and Dr. Paul Reeder were of great importance to the completion of this research.

The guidance and suggestions of Dr. John Rasmussen and Dr. Joseph Cerny are gratefully acknowledged.

Also deserving of mention for their interest and helpful discussions are Dr. Arthur Pape, Mr. David Anderson, Dr. M. Lee Hyder, Dr. John Olmsted, Dr. Richard Pehl, and Mr. John Nash.

Particular gratitude is expressed to the operators and staff of the Hilac, the 80" cyclotron, and the 60" cyclotron for providing the projectile beams and for their help in solving the many problems arising during the experimentation.

Without the services of Mr. Charles Campbell and the electronics repair group this work would not have been possible.

The assistance of the Health Chemistry Group in transporting the targets and in monitoring the chemical separations was appreciated.

Special thanks go to Dr. Eugene Huffman and the members of the analytical group for performing the chemical yield determinations.

Stellar performance by the administration and secretaries of the Nuclear Chemistry Division eased many of the problems arising during this work.

The constant encouragement and assistance of my wife, Ann, made the performance of this research considerably easier, and were invaluable in its completion.

This work was performed under the auspices of the U. S. Atomic Energy Commission.

APPENDIX I. CHEMICAL PROCEDURES—TARGET PREPARATION

A. Nickel^{61} Target

Nickel-61 was obtained as the oxide from Oak Ridge National Laboratory. It was brought into solution by digestion in a solution containing 10 ml of 3 M HNO_3 and 2 ml of 6 M H_2SO_4. This solution was evaporated to dryness, the process repeated, and the solid dissolved in 5% H_2SO_4. NH_4OH was added and the basic solution was diluted to 10 ml.

Two targets were then prepared by electro-deposition of the Ni^{61} on 1/4 mil gold foils. Each was plated from a solution containing 5 ml of the Ni^{61} solution prepared above, 10 ml 6 M NH_4OH and 5 ml H_2O. The plating current was 20 milliamperes (2.4 V) and was maintained for a period of three hours. A smooth, shiny deposit of nickel was obtained which, in each case, was ~ 1.55 mg/cm^2 thick. Thickness was determined from the difference in weight of the gold backing foil before and after plating, and the known area covered by the nickel deposit. The electroplating cell used is shown in Fig. 24.

Solutions remaining from the preparation of the first two targets were combined and evaporated down to ~ 5 ml. This was then used to prepare a third target in the manner already described. Target three was about half as thick as the first two targets (0.74 mg/cm^2).

Mass analysis and spectrographic analysis obtained from Oak Ridge along with the enriched Ni^{61} were used in the calculation of cross sections. These are listed in Table I.

B. Natural Chromium Target

Preparation of the chromium targets was performed using a laboratory version of an industrial chrome-plating cell.[32] The solution used contained 2.5 moles/liter of CrO_3 and 0.025 moles/liter of H_2SO_4. During plating the temperature was maintained between 40° and 50° C., and the bath was gently agitated. The current used was 1.6 amps corresponding to the prescribed current density of 0.16 amps/cm^2 for the 10 cm^2 cathode area used. Typical plating times were 10-15 minutes. The anode was a

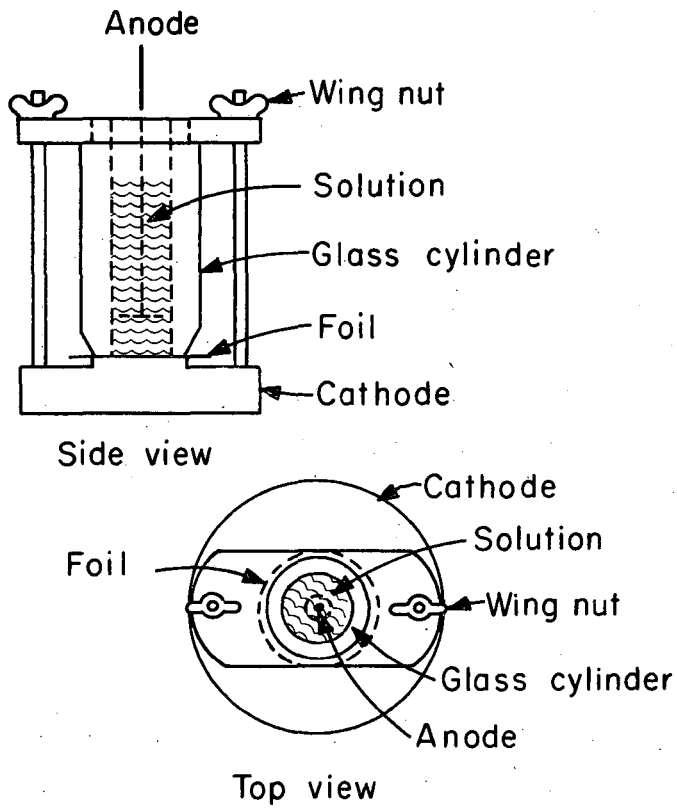

Fig. 24. Electroplating cell used for preparation of the Ni^{61} targets.

1/8-inch lead sheet of nearly the same area as the cathode. A specially constructed cathode was constructed of aluminum and stainless steel. It was designed so that only a 13/16-inch diameter circle of the 1/10 mil gold backing foil (1-inch diameter) was exposed to the solution. The cell design, including details of the cathode, is indicated in Fig. 25. The cell used for Ni plating was not applicable, due to pitting from the large volume of gas generated during Cr plating. The vertical position of the gold foil and constant agitation of the solution overcame this difficulty.

Chromium foils obtained in the above manner were shiny and smooth. There was a tendency to pucker the gold backing foil, but the cathode design minimized this problem. Foils which did pucker during plating were discarded due to the resulting unevenness in their thickness. Early work with Cr plating used 1/4 mil gold foils as backing. For these, the puckering tendency was not noticed, but their thickness proved too great for these experiments.

The CrO_3 used was obtained commercially. Analysis of this material and the mass analysis of natural chromium are included in Table I.

C. Preliminary Experiments

Before preparation of the Ni^{61} and Cr targets, several experiments were performed to determine a satisfactory design for the plating cell, optimum conditions for plating, and uniformity of thickness of the metal deposit.

The cell design and the optimum conditions are, of course, interrelated. Since the electroplating cell used for the Ni^{61} targets was available, it was tried first. The procedure described for nickel plating was adopted, and several trial experiments, starting with NiO, led to the procedures and conditions described earlier in this section. Gold was chosen as the backing foil primarily due to its high Coulomb barrier which prevented activities from He^3 reactions over most of the energy region used.

The procedure chosen for Cr plating is the "weak bath process" used industrially. All attempts using the same cell that was used for Ni

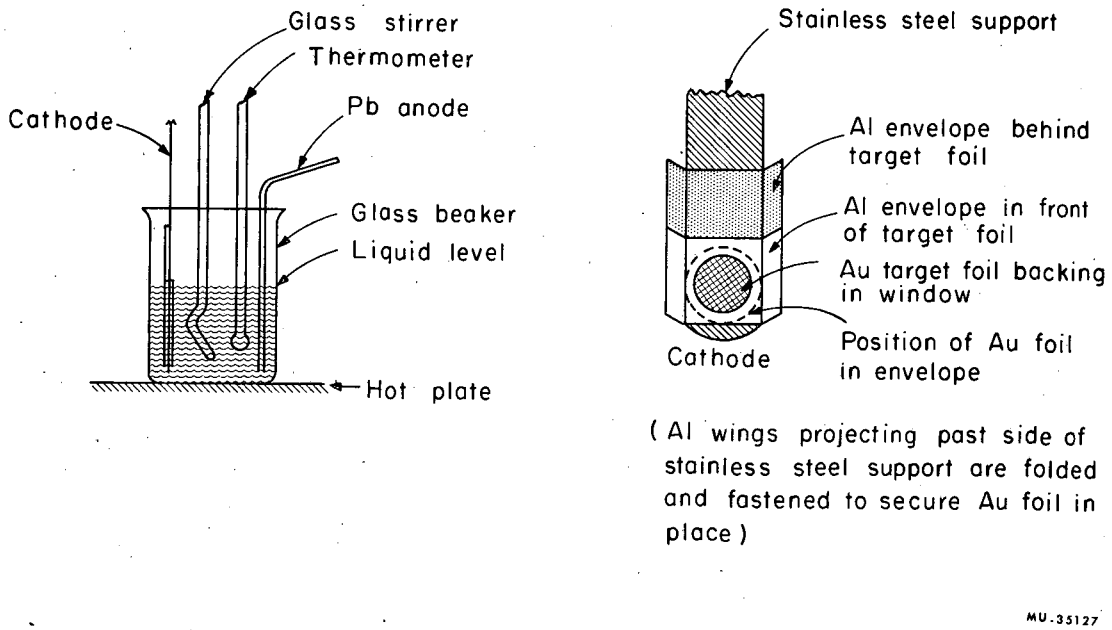

Fig. 25. Electroplating cell used for preparation of the natural chromium targets. Details of the cathode are included.

failed, due to the large volume of gas given off at the cathode and also the difficulty in maintaining a constant elevated temperature. A large (1 liter) bath also failed. It was designed to plate a strip of gold foil 12.5 × 3 cm from which 1-inch circles were cut for possible use as targets. It was found that thicknesses varied rather strongly from one end of the strip to the other. Severe difficulty was also encountered in confining the plating to one side of the gold and in keeping the gold flat during the process. Thus experimental and practical difficulties dictated the adoption of the simple, but functional design shown in Fig. 25.

Uniformity of thickness for both the Ni and Cr deposits were experimentally checked (the nickel by inference from natural nickel deposits). Several representative, potential target foils were cut into sections through the center of the foil. These segments were weighed, the metal deposit dissolved, and the gold backing was weighed again. Ratios of these two weights proved to be the same within about 5%. Some uncertainty is involved in centering the metal deposit on the gold backing. The gold itself is uniform to ~ 2%. Therefore it is estimated that the target foils are uniform to $\leq$ 2%. This is judged quite satisfactory for the present experiment and is only a minor source of uncertainty in the results.

APPENDIX II. DETAILS OF ELECTROMETER CALIBRATIONS

Records of beam intensity during bombardment and of total beam striking the targets were obtained for each irradiation using a conventional integrating beam electrometer connected to the Faraday cup target holder. Effects of secondary electrons or gas ionization were prevented by placing the Faraday cup in a magnetic shield. To eliminate some error in total beam measurement the electrometer was calibrated prior to each bombardment.

A Weston standard cell (1.019 volts) was connected to the input of the electrometer through a precision 10^7 ohm resistor. This current input was recorded for a period of 2.00 minutes and the total observed for this period was related to that calculated by Ohm's law to obtain the correction factor. Duplicate determinations were made. Two successive determinations rarely were in disagreement by more than 0.3% and often less. Overall correction factors determined in this way were usually less than $\pm$ 5%.

APPENDIX III. CHEMICAL PROCEDURES—SAMPLE PREPARATION

The procedures referred to in Sec. II-D are here described in detail. The scheme is designed to separate zinc and copper from the natural chromium and nickel targets and from the aluminum catcher foils used in this investigation. Overall time from end of bombardment to counters had to be kept short. For this reason no attempts were made to optimize chemical yields or to secure ultra pure separated products. In spite of this need for haste, chemical yields were normally around 80%, and the radiochemical purity of the samples was quite good. Separation time was about 5 minutes for copper and somewhat longer for zinc. (Copper samples normally were placed on the counters before zinc was precipitated.)

Chemical Separation Procedures

Flow Sheet

A. Target dissolution

1. Chromium targets (gold backing) and Al catcher:
   a. dissolve in 12 M HCl containing 10 mg Cu^{++} and Zn^{++} as carriers.
   b. rinse Au foil with distilled H_2O into tube.
   c. dip Au foil in warm 6 M HNO_3 to remove any Cu deposited by electrolytic action during dissolution.
   d. remove Au foil from HNO_3, wash and discard.
   e. combine HCl and HNO_3 solutions.
   f. boil to reduce volume to 10 ml or less.
2. Nickel targets and Al catcher:
   a. dissolve in 12 M HCl containing 10 mg Cu^{++} and Zn^{++} as carriers.
   b. add H_2O_2 (30%) and warm to complete dissolution.
   c. heat strongly to destroy excess peroxide.

B. Copper separation

1. To the solution from 1-f or 2-c of part A (above) add conc. NH_4OH carefully until deep blue $Cu(NH_3)_4^{++}$ appears. Zn^{++} is also retained in solution as the ammonia complex.
2. Centrifuge and discard $Al(OH)_3$ precipitate*.
3. Add $Na_2S_2O_4$ crystals to the strongly ammoniacal solution until precipitation of copper metal is complete. Warming in a hot water bath hastens the precipitation.
4. Centrifuge and decant the supernate.
5. Slurry the Cu precipitate, filter, wash with H_2O, EtOH, and acetone, and mount.

C. Zinc separation

1. Add 6 M NaOH to the supernate from step B-4 above and heat to boiling
2. Continue boiling and NaOH additions until the fumes no longer turn moist pH paper dark
3. Adjust the pH with HCl until the solution tests pH 5 to 6. A white precipitate $Zn(OH)_2$ will form and redissolve as the pH = 7-8 point is passed.
4. Add an excess of $(NH_4)_2HPO_4$ and digest the resulting $ZnNH_4PO_4$ precipitate in a boiling water bath.
5. Cool, filter, wash with $(NH_4)_2HPO_4$ solution, water, EtOH, and acetone, and mount.

D. Ion exchange separation (Alternative procedure to parts B and C above and was used for about half the nickel targets. It was discarded in favor of chemical procedures because of time considerations.)

1. Evaporate solution from part 2-c nearly to dryness

---

*This step not only removes Al from the solution, but also effectively scavenges it of minor impurities. About 10% of the Cu and Zn is lost.

2. Add 1 ml 12 M HCl to the cooled test tube and dissolve any particles that may be present.
3. Transfer solution to top of Bio-Rad Anion Exchange Resin column. (Ag 1 - X8, 200 mesh, 10 cm × 0.3 cm equipped with device for applying 3 psi air pressure to top of resin.)
4. Flush column with 3 M HCl to remove Ni, Co and other impurities.
5. Flush column with 1 M HCl and catch effluent containing Cu^{++}.
6. Flush column with 10^{-3} M HCl and catch effluent containing Zn^{++}.
7. Follow steps B-3 to B-5 above to obtain Cu sample using effluent from D-5.
8. Follow steps C-3 to C-5 above (using NH_4OH and/or HCl to adjust the pH) to obtain Zn sample from effluent from step D-6.

APPENDIX IV. DETAILS OF RESOLVING TIME MEASUREMENT

A standard paired source method[85] was used to measure resolving times for each of the beta-counters used in this work. Two approximately equal strength (10^6 disintegrations per minute) Sr^{90} sources were employed. The resolving time, ρ, is given by:

$$\rho = \frac{\delta}{2n_A n_B - 2(\delta + B)n_S - (\delta + B)^2} \tag{31}$$

where n_A = observed count rate of sample A
n_B = observed count rate of sample B
n_S = observed count rate of samples A and B taken together side by side
$\delta = n_A + n_B - n_S - B$
B = background

It is important that contributions to the counting rate not be effected by geometry changes. Therefore, the counts should be taken in the order n_A, n_S, n_B. This insures that samples A and B retain the same geometry when counted separately or together. Eq. 31 is often simplified by retaining dominant terms only, and becomes:

$$\rho = \frac{\delta}{2n_A n_B} \tag{32}$$

The limiting component of the beta counters is the scaling circuit. This instrument is classified as a non-polarizable apparatus and fits into the type II counting circuits described by Evans.[85] With the assumption that the resolving time is much less than the observation time of the measurement, the true counting rate (N) is given by

$$N = \frac{n}{1 - n\rho} \tag{33}$$

The function $1/1 - n\rho$ is plotted versus n in Fig. 26 for each of the counters involved and can be used to obtain the corrections referred to in the experimental description in Sec. II-E.

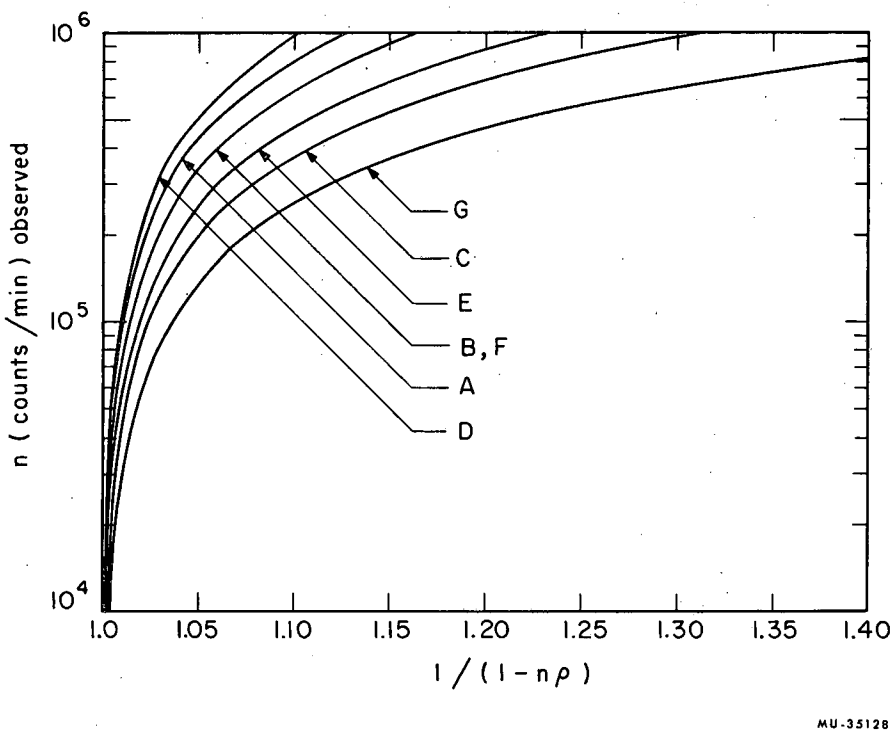

Fig. 26. Beta counter resolving time correction as a function of observed counting rate. The letters designate the particular beta counter corresponding to a given curve.

Values of ρ were measured to better than $\pm$ 15% uncertainty. The resulting error in the correction factor will therefore be $\pm$ 2% at most. Furthermore, the count rates were not allowed to approach a magnitude such that resolving time corrections exceeded 10%. The overall error induced in the cross section measurements by virtue of this correction was, therefore, only about $\pm$ 2% at most. Most of the data did not require the application of a dead time correction. The experimental averages for resolving time with their associated errors appear in Table IX. Also included there are typical values and errors for the correction, $1/1 - n\rho$, and the corresponding true counting rate.

Table IX. Beta counter resolving time correction.

Counter	Resolving time, ρ, (μs)	Correction factor at 5×10^5 cpm
A	6.9 ± 0.5	1.062
B	8.4 ± 0.8	1.076
C	14 ± 1.8	1.135
D	5.6 ± 0.7	1.048
E	11.3 ± 0.3	1.102
F	8.6 ± 0.2	1.076
G	20 ± 1.1	1.21

APPENDIX V. DETAILS OF OVERALL DETECTION COEFFICIENT DETERMINATIONS

An overall detection coefficient, representing the ratio of observed activity to absolute disintegrations per minute was experimentally determined for each of the counter-shelf-nuclide combinations used. Application of such a procedure eliminates the need for separate evaluations of corrections due to geometry, backscatter, scatter from counter walls, detection probability, window absorption, etc. A chemically separated weightless sample of the nuclide to be used was mounted on a thin gold-coated VYNS film[86] and counted in a standardized 4π beta proportional counter to obtain its absolute activity. The same sample was then mounted on an aluminum card in the same manner as was used in mounting ordinary samples and was counted on the various shelves of as many counters as the half life would permit. Count rates were then corrected for decay during measurements. Each combination was repeated three times. The ratio of observed count rate to absolute activity is averaged for each shelf and counter and this average is the experimental counting efficiency for positrons, $E_{\beta+}$. Normally, a self-absorption coefficient would also be needed, but the high energy of the $\beta+$ particles involved made this appear unnecessary.

Nevertheless, experimental attempts to measure self-absorption were carried out using the procedures outlined by Pate and Yaffe.[87] No change of activity was detected when samples, identical except for increasing thickness up to 30 mg/cm^2, were counted. Sample thickness was only 10 mg/cm^2 maximum during the experiment so no self-absorption correction was required.

The overall detection coefficient, ODC, is the product of the experimental counting efficiencies and the fraction of the total number of disintegrations that give observable events. This fraction is obtained from the decay schemes of the various nuclei, and is simply the branching ratio in the cases of Zn^{63} and Cu^{62}, since the decay of these nuclei produces a stable daughter. In the case of Zn^{62} the daughter is Cu^{62}, a radioactive nucleus, and because of the relationship of the half lives a state of transient equilibrium is established. Therefore the activity

from both parent and daughter must be considered. Every decay of a Zn^{62} nucleus produces a Cu^{62}, but only 10% of these decays proceed via beta emission. Thus the fraction of observable events to total decays is 1.10 for Zn^{62}. Because of this transient equilibrium it was always necessary to allow enough time for the daughter to grow in before counting chemically separated zinc samples. However, because of the short bombardment times and reasonably rapid elapsed time between bombardment and chemical separation, there was a maximum production of Cu^{62} from Zn^{62} decay which was less than 0.1% of the Cu^{62} produced directly by (x,pn) reactions. Therefore, the daughter nuclei that were separated chemically and included with the Cu^{62} product were ignored.

The overall experimental uncertainty is about $\pm$ 2% due primarily to counting statistics. Averaging reduces this value somewhat, but other uncertainties (i.e., 4π counter standardization, possible radioactive impurities, branching ratios, etc.) tend to counteract this averaging. Table III gives the branching ratios used in this work, while the overall detection coefficients are listed for some typical geometries of the various counters in Table X.

Table X. Overall detection coefficients.

Counter	Cl^{36} standard normalization (cpm)	Shelf	$ODC_{(Zn^{62})}$	$ODC_{(Zn^{63})}$	$ODC_{(Cu^{62})}$
A	63500	3	0.229	0.210	0.208
		7	0.0276	0.0233	0.0251
		9	0.0118	0.0097	0.0107
B	63500	3	0.230	0.210	0.209
		7	0.0276	0.0252	0.0251
		9	0.0119	0.0107	0.0108
C	63500	3	0.232	0.208	0.211
		7	0.0272	0.0244	0.0247
		9	0.0115	0.0101	0.0105
D	63500	3	0.226	0.207	0.206
		7	0.0272	0.0252	0.0247
		9	0.0124	0.0110	0.0113
F	63500	3	0.238	0.201	0.216
		7	0.0292	0.0244	0.0266
		9	0.0135	0.0104	0.0123
G	65000	3	0.238	0.203	0.216
		7	0.0304	0.0255	0.0276
		9	0.0138	0.0110	0.0126

APPENDIX VI. ANALYSIS OF ERRORS IN THE EXPERIMENTAL RESULTS

A. Errors in Energy Determination

1. Beam Spread

The principal uncertainty in energy values comes from initial beam spread. Full width at half maximum spread is quoted as ± 2% by Hubbard et al.[34] for a typical Hilac beam. The beam spread of the 60-inch cyclotron is of similar magnitude.[33] Presumably the bending magnets used to direct the beams to the targets would lower this spread somewhat but no attempt to evaluate true beam spread at the target has been made. Therefore, the ± 2% estimate should be taken as an upper limit.

The 88-inch cyclotron beam is mono-energetic by the above standard, but as no measurement of its energy was made, it is the week-to-week variation in energy that provides the uncertainty limits. This variation has been estimated as ± 2%, a conservative value, and is adopted as the range of possible beam energies for the proton bombardments.

2. Degradation

In addition to the spread in the initial beam energy, there is an additional uncertainty due to degradation-induced spread as the beam traverses the foil stack. According to McIntyre et al.[88,89] the energy spread due to degradation increases as the ratio of stopping powers after and before such degradation. With the stopping power curves as given by Northcliffe,[37] this increase amounts to a factor of 2.5 to 3 for the ions used in this work over a loss in energy from 10 MeV/Amu to the Coulomb barriers of the targets (~ 2-3 MeV/Amu). Thus overall uncertainty in beam energy increases from less than ± 2% for the first foil to about ± 5% for the last foil of the target.

Energy spread for the proton beam may be estimated from the stopping power curves for protons in aluminum published in Nuclear Data Tables. The spread is found to increase by a factor of four in degrading a 30 MeV beam to 5 MeV. If the initial beam spread is taken to be small with the uncertainty in absolute energy within 2% of 30.0 MeV, then at the Coulomb barrier, the uncertainty in the beam energy will be on the order of 5%.

3. Other Sources

Other possible sources of error in energy determinations are the foil thicknesses and the range-energy curves. Fortunately, any errors in measurements stemming from these causes will be small due to their tendency to cancel each other. Such cancellation is expected because, in the first case, many foils of random orientation with respect to each other were used to construct the target stack, and in the second case, because only differences in ranges or energies were used. Thus, these sources of possible error are much less than that due to beam spread, and only the latter is reflected in the errors listed in Table XI and presented as error bars with the experimental data in Figs. 5, 7, 9, and 10.

B. Errors in Cross Section Measurements

1. General Considerations

Calculations of values for cross sections involve several different experimentally measured quantities. As was the case for the range-energy curves, the "best" literature values for the half lives of all nuclides involved in this work were assumed accurate and no attempt at assigning an uncertainty range was made. The values used are included in Table III. Furthermore, time measurements were better than ± 1% and therefore will be ignored as an error source. Principal sources of error are, therefore, assumed to include only the terms of Eq. 2 representing particle flux, target thickness, and product disintegrations at end of bombardment. The latter is by far the largest single source of error in this work.

2. Flux

The first of these, particle flux, was measured using a magnetically shielded Faraday cup and an integrating beam electrometer which could be read to ± 1% or less. Furthermore, the electrometer was calibrated prior to each bombardment. This correction factor was measured to better than 1% and rarely affected the electrometer reading by more than 3%. It is therefore felt that the number of particles passing through the target is known to ~ ± 1%.

3. Thickness

the quantity n, target atoms per cm^2, is dependent upon the mass analyses, the accuracy in weighing the target foils, and their uniformity. Possible errors in the mass analyses are ignored. Weighing was accomplished to an accuracy of ± 1% for thinnest foils, the error being less for the thicker foils. The Ni^{61} and Cr targets were weighed by difference in weight of the gold foils before and after electroplating. These weighings were made on a micro-balance, and errors were thereby held to ± 1% or less. Areas of the foils are known to 0.1% because a precision punch was used to cut them. Uniformity of thickness across the foils was quite good, being taken as ± 1.4% for the natural Ni foils from the manufacturer's statement and estimated as less than ± 3% for the electrodeposited targets Ni^{61} and Cr. The overall error to be attached to n, target atoms per square centimeter, is therefore on the order of ± 2%.

4. Disintegration Rate

The number of product nuclei disintegrations per minute at the end of bombardment (D_0) is itself a calculated value, with errors being due to several sources. The primary experimental quantity is A_0, the activity at end of bombardment. Uncertainty in this measurement was calculated (as the standard deviation) by the FRENIC computer program, or simply estimated by noting the range over which a straight line could be drawn through the experimental points. The two procedures, when applied to the same set of data, gave very nearly the same result. Since decay curve analysis involves a series of subtractions the inherent errors tended to compound themselves as components were successively subtracted from the raw curve. In the general case, no large errors were introduced by this subtraction because the components were characterized by sufficiently different half lives to that reliance upon points obtained by subtraction of two large numbers to obtain a small one was not necessary. On the contrary, points determining the position of a component on the curve normally comprised 60% or more of the activity represented by the original curve before subtraction.

All counts were taken with the aid of the "pipper" described in Sec. II. Thus three place accuracy was the rule, and the measured count rate was known to ± 1% at worst. Counting statistics were also ± 1% or less, by virtue of increased counting time and scaling factor adjustments. Background, while normally amounting to less than 10% of the activity, was known to 1% with day to day variations amounting to less than 1%. It was therefore reasonable to find that the first, or longest lived, component could be positioned on the curve with an accuracy of ± 2-3%. Typical errors experimentally assigned to A_0 measurements are listed in Table XI. The increase in error with decreasing half life is due to the compounding of errors described above and closely follows the expected trend estimated from purely statistical considerations.

To calculate disintegration rate from activity, correction factors for counting efficiency, branching ratio, chemical yield, and counter dead time are used. The counting efficiency and dead time correction are both experimentally measured to ± 2% or better. Chemical yield uncertainties amount to less than 2%. The fraction of decays going by positron emission is ignored as a possible source of error. Values used are listed in Table III for reference.

5. Summary

It is therefore seen that all these factors are only minor sources or error in these cross section calculations as compared to the A_0 determination. Combining the errors listed in previous paragraphs as if they were standard deviations insures a conservative estimate of the overall uncertainty. Values obtained in this manner from the above figures complete Table XI and are used in graphing the vertical error bars of Figs. 5, 7, 9, and 10.

An actual count of the number of points differing from the experimental curves by more than these estimated deviations was taken. For the Zn^{62} and Zn^{63} curves this number was 35% of the total number of points. For Cu^{62} this number was 23% of the total. For true standard deviations the number of points falling off the curves is 32%. The agreement is encouraging and implies that the above are reasonable estimates of the errors involved.

Table XI. Estimation of experimental errors.

Error source	Isotope		
Energy determinations	Zn^{63}	Zn^{62}	Cu^{62}
Beam spread	± 2%	± 2%	± 2%
Energy degradation	± 5% max ...		
Foil thickness variations	small ...		
Range energy	assumed zero		
Foil thickness (energy uncertainty)	variable ...		
Expected uncertainty in energy	± 2 to ± 5% exclusive of finite target thickness		
Cross section determinations			
Half lives, time measurements and branching ratios	considered negligible		
Flux measurement	± 1%	± 1%	± 1%
Target thickness	± 2%	± 2%	± 2%
Disintegration rate	± 6%	± 3%	± 8%
Expected uncertainty in cross sections	7%	4%	8%

REFERENCES

1. J. Chadwick, Nature 129, 312 (1932).
2. N. Bohr, Nature 137, 344 (1936).
3. V. F. Weisskopf, Phys. Rev. 52, 295 (1937).
4. H. A. Bethe, Revs. Mod. Phys. 9, 69 (1937).
5. J. Blatt and V. F. Weisskopf, Theoretical Nuclear Physics (John Wiley and Sons, Inc., New York 1952).
6. K. J. LeCouteur, Nuclear Reactions (edited by P. M. Endt and M. Demeur, North Holland Pub. Co., Amsterdam, 1959).
7. T. Ericson, Advances in Physics 9, 425 (1960).
8. H. Feshbach, Nuclear Spectroscopy, Part B (F. Ajzenberg-Selove, Ed., Academic Press, New York, 1960).
9. D. Bodansky, Ann. Rev. Nucl. Sci. 12, 79 (1962).
10. S. N. Ghoshal, Phys. Rev. 80, 939 (1950).
11. J. W. Meadows, Phys. Rev. 91, 885 (1953).
12. S. Tanaka, J. Phys. Soc. Japan 15, 2159 (1960).
13. F. K. McGowan, P. H. Stelson, and W. G. Smith, Bull. Am. Phys. Soc. II 5, 266 (1960).
14. H. A. Howe, Phys. Rev. 109, 2083 (1960).
15. J. P. Blaser, F. Boehm, P. Marmier and D. C. Peaslee, Helv. Phys. Acta 24, 3 (1951).
16. B. L. Cohen and E. Newman, Phys. Rev. 99, 718 (1955); Cohen, Newman, and Handley, Phys. Rev. 94, 620 (1954).
17. W. John, Phys. Rev. 103, 704 (1956).
18. J. W. Meadows and R. B. Holt, Phys. Rev. 83, 47 (1951).
19. M. A. Tamers and R. Wolfgang, Phys. Rev. 117, 812 (1960).
20. B. L. Cohen, H. L. Reynolds, and A. Zucker, Phys. Rev. 96, 1617 (1954).
21. N. M. Hintz and N. F. Ramsey, Phys. Rev. 88, 19 (1952).
22. K. L. Chen and J. M. Miller, Phys. Rev. 134, B1269 (1964).
23. R. A. Sharp, R. M. Diamond, and G. Wilkinson, Phys. Rev. 101, 1493 (1956).
24. S. Tanaka, M. Furukawa, S. Iwata, M. Yagi, H. Amano, and T. Mikumo, J. Phys. Soc. Japan 15, 2125 (1960).

25. C. M. Stearns, Comparison of Reactions of Copper-63 Compound Nuclei Formed by Alpha-particle, Proton, and Carbon-ion Bombardments (Ph. D. Thesis), NYO-10387 (1962).

26. N. T. Porile, S. Tanaka, H. Amano, M. Furukawa, S. Iwata, and M. Yaki, Nucl. Phys. 43, 500 (1963).

27. J. R. Grover and R. J. Nagle, Phys. Rev. 134, B1248 (1964).

28. W. J. Nicholson, Jr., Measurements Relating to the Height of the Fission Barrier in Elements Lighter than Thorium (Ph. D. Thesis), University of Washington, Seattle, Washington (1960).

29. T. Kammuri and R. Nakasima, Proc. Second Intern. Conf. Reactions between Complex Nuclei, Gatlinburg (John Wiley and Sons, Inc., New York, 1960), p. 301.

30. T. Kammuri, Prog. Theoret. Phys. 25, 235 (1961).

31. G. R. Keepin, T. F. Wimelt, and R. K. Zeigler, J. Nucl. Energy 6, 1 (1957).

32. H. Silman, Chemical and Electro-plated Finishes, (Chapman and Hall, Ltd., London, 1952), p. 321.

33. T. D. Thomas, Lawrence Radiation Laboratory Report UCRL-3791, 1957 (unpublished).

34. E. L. Hubbard, et al., Rev. Sci. Instr. 32, 621 (1961).

35. R. M. Sternheimer, Phys. Rev. 117, 485 (1960).

36. H. Bischel, Phys. Rev. 112, 1089 (1958).

37. L. C. Northcliffe, Ann. Rev. Nucl. Sci. 13, 67 (1963); NAS-NRC Series, Report No. 8.

38. C. Williamson and J. P. Boujot, Centre D'Etudes Nucleaires de Saclay, CEA 2189 (1962).

39. J. Lindhard, M. Scharff, and H. E. Schiøtt, Kgl. Danske Videnskab. Selskab, Mat.-Fys. Medd. 33, No. 14 (1963).

40. H. M. Blann, (Ph. D. Thesis), Lawrence Radiation Laboratory Report UCRL-9190, 1960.

41. P. L. Reeder, (Ph. D. Thesis), Lawrence Radiation Laboratory Report UCRL-10531, 1962.

42. R. W. Hayward, Phys. Rev. 79, 541 (1950).

43. R. A. Ricci, R. K. Girgis, R. van Lieshout, Nuovo Cimento 11, 156 (1959).
44. J. W. Butler and C. R. Grosset, Phys. Rev. 112, 1257 (1958).
45. G. Friedlander and J. W. Kennedy, Nuclear and Radiochemistry, (John Wiley and Sons, Inc., New York, 1955).
46. F. S. Houck and J. M. Miller, Phys. Rev. 123, 231 (1961).
47. D. J. Reuland, N. K. Ganguly, and A. A. Caretto, Jr., Phys. Rev. 133, B1171 (1964).
48. S. S. Markowitz, J. M. Miller, and G. Friedlander, Phys. Rev. 98, 1197 (1955).
49. E. A. Bryant, D. R. F. Cochran, J. D. Knight, Phys. Rev. 130, 1512 (1963).
50. J. B. Read, I. M. Ladenbauer-Bellis, R. Wolfgang, Phys. Rev. 127, 1722 (1962).
51. I. M. Ladenbauer-Bellis, I. L. Preiss, and C. E. Anderson, Phys. Rev. 125, 606 (1962).
52. A. S. Karamyan, Y. B. Gerlit, B. F. Myasoedov, J. Exptl. Theoret. Phys. USSR 36, 621 (1959).
53. J. M. Alexander and L. Winsberg, Phys. Rev. 121, 529 (1961).
54. J. M. Alexander and D. H. Sisson, Phys. Rev. 128, 2288 (1962).
55. M. Kaplan and R. D. Fink, Phys. Rev. 134, B30 (1964); M. Kaplan, Phys. Rev. 134, B37 (1964).
56. M. Blann and A. Ewart, Phys. Rev. 134, B783 (1964).
57. B. G. Harvey, Ann. Rev. Nucl. Sci. 10, 235 (1960).
58. R. Pehl, private communication.
59. P. E. Hodgson, Proceedings of the Conference on Direct Interactions and Nuclear Reaction Mechanisms, University of Padua (Gordon and Breach, New York, 1963), p.103.
60. P. E. Hodgson, The Optical Model of Elastic Scattering, (Clarendon Press, Oxford, 1963), p. 102.
61. P. E. Hodgson, ibid., p. 127.
62. R. H. Bassel, G. R. Satchler, R. M. Drisko, E. Rost, Phys. Rev. 128, 2693 (1962).

63. R. H. Bassel, International Conference on Nuclear Structure, Queens University, Kingston, Ontario, 1960 (D. A. Bromley and E. W. Voight, U. of Toronto Press, Toronto) p. 212.
64. W. L. Hafner, Jr., J. R. Juizenga, and R. Vandenbosch, Computer Program for Calculating the Relative Yields of Isomers Produced in Nuclear Reactions, ANL-6662 (1960).
65. 1960 Nuclear Data Tables, National Academy of Sciences-National Research Council, Washington, D. C., (1961), Part 1.
66. R. Sagane, Phys. Rev. 85, 926 (1952).
67. J. F. Mollenauer, (Ph. D. Thesis), Lawrence Radiation Laboratory Report UCRL-9724, June 1960 (unpublished).
68. G. N. Simonoff and J. M. Alexander, Lawrence Radiation Laboratory Report UCRL-10099, February 1962 (unpublished).
69. J. M. Alexander and G. N. Simonoff, Lawrence Radiation Laboratory Report UCRL-10541, January 1963 (unpublished).
70. R. Vandenbosch and J. R. Huizenga, Phys. Rev. 120, 1313 (1960).
71. F. Fukuzawa, J. Phys. Soc. Japan 16, 2371 (1961).
72. E. Weigold and R. N. Glover, Nucl. Phys. 32, 106 (1962).
73. T. Ericson and V. M. Strutinski, Nucl. Phys. 8, 284 (1958).
74. G. S. Pik-Pichak, Soviet Phys. JETP 11, 557 (1959).
75. M. L. Halbert and F. E. Durham, 3rd Conference on Reactions between Complex Nuclei, Asilomar (University of California Press, Berkeley, 1963), p. 223.
76. D. Sperber, ibid., p. 379.
77. I. Dostrovsky, Z. Fraenkel, and G. Friedlander, Phys. Rev. 116, 683 (1959).
78. J. D. Jackson, Can. J. Phys. 34, 767 (1956).
79. T. Sikkeland, S. G. Thompson, and A. Ghiorso, Phys. Rev. 112, 543 (1958).
80. Tables of the Incomplete Γ-Function, Ed., E. S. Pearson, (Cambridge University Press, London, 1946).
81. G. Igo, Phys. Rev. 106, 256 (1957).
82. G. Igo and H. E. Wegner, Phys. Rev. 102, 1364 (1956).

83. R. M. Eisberg, G. Igo, and H. E. Wegner, Phys. Rev. 100, 1309 (1955).
84. E. L. Kelly, Lawrence Radiation Laboratory Report UCRL-1044, 1950 (unpublished).
85. R. D. Evans, The Atomic Nucleus, (McGraw-Hill Book Company, Inc., New York 1955), p. 789.
86. B. D. Pate and L. Yaffe, Can. J. Chem. 33, 15 (1955).
87. B. D. Pate and L. Yaffe, Can. J. Chem. 33, 929 (1955).
88. J. A. McIntyre, T. L. Watts, and F. C. Jobes, Nucl. Instr. Methods 21, 281 (1963).
89. L. C. Becker, G. K. Tandon, F. C. Jobes, J. A. McIntyre, and T. L. Watts, ibid., p. 298.

This report was prepared as an account of Government sponsored work. Neither the United States, nor the Commission, nor any person acting on behalf of the Commission:

A. Makes any warranty or representation, expressed or implied, with respect to the accuracy, completeness, or usefulness of the information contained in this report, or that the use of any information, apparatus, method, or process disclosed in this report may not infringe privately owned rights; or

B. Assumes any liabilities with respect to the use of, or for damages resulting from the use of any information, apparatus, method, or process disclosed in this report.

As used in the above, "person acting on behalf of the Commission" includes any employee or contractor of the Commission, or employee of such contractor, to the extent that such employee or contractor of the Commission, or employee of such contractor prepares, disseminates, or provides access to, any information pursuant to his employment or contract with the Commission, or his employment with such contractor.